Article

Cell Reports

Cry2 Is Critical for Circadian Regulation of Myogenic Differentiation by Bclaf1-Mediated mRNA Stabilization of Cyclin D1 and Tmem176b

Graphical Abstract

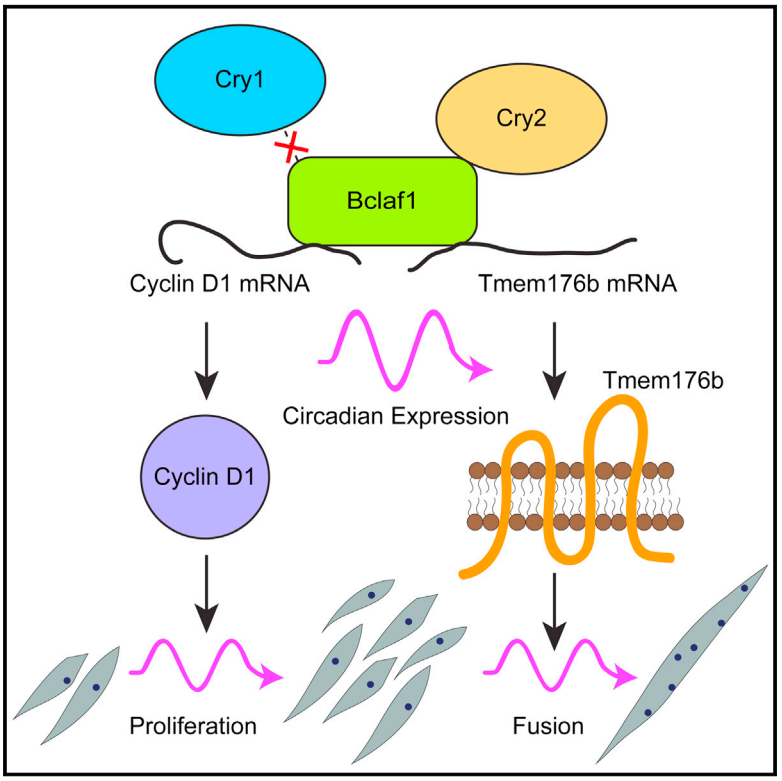

Authors

Matthew Lowe, Jacob Lage, Ellen Paatela, ..., Michaela Lohman, Atsushi Asakura, Nobuaki Kikyo

Correspondence

asakura@umn.edu (A.A.), kikyo001@umn.edu (N.K.)

In Brief

Lowe et al. demonstrates that the core circadian regulator Cry2 interacts with Bclaf1, controlling circadian expression of cyclin D1 and Tmem176b mRNAs. This promotes myoblast proliferation and subsequent myocyte fusion to form myotubes in a circadian manner. This study highlights circadian regulation of myogenic differentiation and regeneration.

Highlights

- Circadian regulator Cry2 promotes muscle cell differentiation and regeneration
- Cry2-Bclaf1 controls circadian DNA synthesis via cyclin D1 mRNA stabilization
- Cry2-Bclaf1 promotes circadian myocyte fusion by stabilizing Tmem176b mRNA
- Bclaf1 depletion recapitulates Cry2 depletion phenotypes in muscle differentiation

Data and Software Availability

GSE100898

Lowe et al., 2018, Cell Reports 22, 2118–2132
February 20, 2018
https://doi.org/10.1016/j.celrep.2018.01.077

CellPress

OPEN ACCESS
CellPress

Cell Reports
Article

Cry2 Is Critical for Circadian Regulation of Myogenic Differentiation by Bclaf1-Mediated mRNA Stabilization of Cyclin D1 and Tmem176b

Matthew Lowe,[1,2,5,7] Jacob Lage,[1,2,7] Ellen Paatela,[1] Dane Munson,[1] Reilly Hostager,[1] Ce Yuan,[1,3] Nobuko Katoku-Kikyo,[1,4] Mercedes Ruiz-Estevez,[1,2] Yoko Asakura,[1,2] James Staats,[1,2] Mulan Qahar,[1,4] Michaela Lohman,[1,6] Atsushi Asakura,[1,4,*] and Nobuaki Kikyo[1,2,8,*]

[1]Stem Cell Institute
[2]Department of Genetics, Cell Biology, and Development
[3]Bioinformatics and Computational Biology Graduate Program
[4]Department of Neurology
University of Minnesota, Minneapolis, MN 55455, USA
[5]Present address: The Molecular Biology IDP, University of California, Los Angeles, Los Angeles, CA 90095, USA
[6]Present address: College of Veterinary Medicine, Michigan State University, East Lansing, MI 48824, USA
[7]These authors contributed equally
[8]Lead Contact
*Correspondence: asakura@umn.edu (A.A.), kikyo001@umn.edu (N.K.)
https://doi.org/10.1016/j.celrep.2018.01.077

SUMMARY

Circadian rhythms regulate cell proliferation and differentiation; however, little is known about their roles in myogenic differentiation. Our synchronized differentiation studies demonstrate that myoblast proliferation and subsequent myotube formation by cell fusion occur in circadian manners. We found that one of the core regulators of circadian rhythms, Cry2, but not Cry1, is critical for the circadian patterns of these two critical steps in myogenic differentiation. This is achieved through the specific interaction between Cry2 and Bclaf1, which stabilizes mRNAs encoding cyclin D1, a G1/S phase transition regulator, and Tmem176b, a transmembrane regulator for myogenic cell fusion. Myoblasts lacking Cry2 display premature cell cycle exit and form short myotubes because of inefficient cell fusion. Consistently, muscle regeneration is impaired in *Cry2*$^{-/-}$ mice. *Bclaf1* knockdown recapitulated the phenotypes of *Cry2* knockdown: early cell cycle exit and inefficient cell fusion. This study uncovers a post-transcriptional regulation of myogenic differentiation by circadian rhythms.

INTRODUCTION

Circadian rhythms regulate the expression of up to 20% of all genes in the body, controlling diverse aspects of cell physiology and pathology, including cell proliferation, stem cell functions, and tissue regeneration (Lowrey and Takahashi, 2011; Plikus et al., 2015; Takahashi, 2017). Mammalian circadian rhythms are organized by the suprachiasmatic nucleus (SCN) in the hypothalamus. Light stimulation received by the retina is transmitted to the SCN, which then synchronizes the circadian rhythms of body temperature, sleep/awake, and other physiological regulations through hormones and the autonomic nervous system. Disruption of the SCN causes desynchronization of circadian rhythms in the body, but the rhythms persist at a single-cell level because of the intrinsic and ubiquitous Clock/Bmal1 feedback system. This system allows isolated cells to autonomously maintain circadian rhythms *in vitro*.

At the core of circadian gene regulation lies the auto-regulatory loop centered on the Clock/Bmal1 transcription factor complex (Buhr and Takahashi, 2013; Hirano et al., 2016; Takahashi, 2017). The oscillating expression level of *Bmal1* generally reaches the highest level during light-on hours and the lowest level during light-off hours *in vivo*. The two basic-helix-loop-helix Per-Arnt-Sim (PAS) transcription factors Clock and Bmal1 form a heterodimer and activate target genes, including *Cry1*, *Cry2*, *Per1*, and *Per2*, through binding to the E-box (5′-CANNTG-3′) in their promoters. Cry and Per proteins then heterodimerize and inhibit the Clock/Bmal1 complex, forming the first negative feedback loop. Cry and Per proteins subsequently undergo phosphorylation and ubiquitination, leading to degradation by the proteasomal pathway. This degradation relieves Clock/Bmal1 from the negative feedback loop and restarts the next cycle of Clock/Bmal1-stimulated gene activation. Clock/Bmal1 also activates the transcription of genes encoding RORα (retinoic acid receptor-related orphan receptor α), RORβ, and RORγ as well as Rev-erbα (reverse orientation c-erbAα) and Rev-erbβ. RORs activate but Rev-erbs inhibit the transcription of *Bmal1* through competition for binding sites at the promoter of *Bmal1*, providing the second feedback loop of circadian rhythms. These feedback loops exist in almost all tissues examined.

Mouse Cry1 and Cry2 proteins contain 606 and 592 amino acids, respectively, and share 89.4% similarity at the amino acid level. *Cry1*$^{-/-}$ and *Cry2*$^{-/-}$ mice are fertile without any gross morphological abnormalities and can sustain circadian rhythms (van der Horst et al., 1999; Vitaterna et al., 1999). In contrast,

Cry1$^{-/-}$ *Cry2*$^{-/-}$ double knockout (KO) mice completely lose the rhythms, indicating the presence of functional redundancy between the two genes. However, several findings indicate that Cry1 and Cry2 cannot completely compensate for each other. For example, although the circadian period of *Cry1*$^{-/-}$ mice is around 23 hr, that of *Cry2*$^{-/-}$ mice is around 25 hr (Thresher et al., 1998; van der Horst et al., 1999). In addition, inactivation of *Cry2*, but not *Cry1*, can restore lost circadian rhythms in *Per2* partial deletion mutant mice (Oster et al., 2002). Furthermore, only Cry2 serves as a component of an E3 ligase complex that ubiquitinates c-Myc prior to its degradation (Huber et al., 2016). Specific molecular interactions underlying these differences remain largely elusive.

Circadian rhythms control the expression of genes encoding cell cycle regulators, including p21 (*Cdkn1a*), cyclin D1 (*Ccnd1*), and c-Myc (Soták et al., 2014). This oscillating expression controls circadian phase-specific cell proliferation in a tissue-specific manner. Although DNA replication reaches the maximum level in late afternoon in human keratinocytes (Geyfman et al., 2012), it reaches a peak in early morning in human rectal epithelial cells (Buchi et al., 1991). Cell differentiation is also regulated by circadian rhythms in a tissue-specific manner (Janich et al., 2014). For example, knockdown (KD) of *Clock* or *Per2* inhibits differentiation of mesenchymal stem cells into adipocytes but not into osteoblasts (Boucher et al., 2016). Epidermal stem cells express genes important for differentiation and organelle biogenesis in a circadian manner (Janich et al., 2013). Progression of hair follicle cycling is delayed by disruption of *Clock* or *Bmal1* in mice (Lin et al., 2009).

Adult skeletal muscle regeneration is mediated by myogenic stem cells, called satellite cells, which are mitotically quiescent in adult muscle (Motohashi and Asakura, 2014). However, they initiate proliferation upon stimulation by weight bearing or through damage. The progenies of activated satellite cells, now called myoblasts, undergo multiple rounds of cell division prior to terminal differentiation. The cells that have exited from the cell cycle, called myocytes, form multinucleated myotubes by cell fusion. During maturation, myotubes continuously enlarge through additional myocyte fusion as well as increased cytoplasmic volume per nucleus, resulting in functional myofibers with the capability of contraction. Aging and various diseases impair the capacities of muscle regeneration, including satellite cell proliferation, self-renewal, and myogenic differentiation, resulting in dystrophic and atrophic muscle (Saini et al., 2016).

In mouse skeletal muscle, more than 2,000 genes are expressed in a circadian manner (Harfmann et al., 2015; Pizarro et al., 2013). The Clock/Bmal1 complex binds to the E-box in the core enhancer of the *MyoD* gene and induces circadian oscillation of *MyoD* expression (Andrews et al., 2010; Lefta et al., 2011). Deletion of the mouse *Clock* or *Bmal1* gene abolishes *MyoD* oscillation and disrupts myofilament architecture and contractile force. Consistent with this *MyoD* regulation, decreased expression of *Bmal1* disrupts the differentiation of myoblasts to myotubes, which can be explained by impaired Wnt signaling (Chatterjee et al., 2013). Currently, virtually nothing is known about the specific contributions of Cry and Per to myogenic differentiation and muscle regeneration.

The present study focuses on the differential roles of Cry1 and Cry2 in the differentiation of mouse myoblasts to myotubes *in vitro* and muscle regeneration *in vivo*. This study unexpectedly uncovered that Cry2 promotes cell cycle exit of myoblasts and myocyte fusion during differentiation.

RESULTS

Opposing Effects of *Cry1* and *Cry2* KO on Muscle Regeneration

Both *Cry1*$^{-/-}$ and *Cry2*$^{-/-}$ mice appeared healthy without any obvious skeletal muscle defects. To understand whether there were any differences in the capacity for muscle regeneration between these KO mice, we damaged the *tibialis anterior* (TA) muscle by intramuscular injection of barium chloride. We then examined regeneration with immunofluorescence staining of embryonic myosin heavy chain (eMHC), an early marker for regenerating myofibers, and H&E staining. This study revealed that *Cry1* KO accelerated, whereas *Cry2* KO delayed, muscle regeneration compared with wild-type (WT) TA muscle. Specifically, on day 3 after injection, *Cry1*$^{-/-}$ TA muscle contained more regenerating myofibers expressing eMHC than WT TA muscle, whereas such myofibers were rare in *Cry2*$^{-/-}$ TA muscle (Figures 1A and 1B). On day 4, eMHC(+) myofibers were larger in *Cry1*$^{-/-}$ and smaller in *Cry2*$^{-/-}$ TA muscle relative to the WT (Figure 1C). On day 5, eMHC became almost undetectable in WT and *Cry1*$^{-/-}$ TA muscle but remained abundant in *Cry2*$^{-/-}$ TA muscle (Figure 1A). H&E staining of day 7 TA muscle showed that *Cry1*$^{-/-}$ myofibers were larger but *Cry2*$^{-/-}$ myofibers were smaller than their WT counterparts (Figures 1D and 1E). Phenotypic differences between each strain were already evident in uninjected adult TA muscle. H&E staining showed that myofibers were slightly larger in *Cry1*$^{-/-}$ TA muscle than in WT TA muscle. *Cry2*$^{-/-}$ TA muscle followed a bimodal distribution, and the average size was smaller than WT TA muscle, except for a particularly large population (Figures 1F and 1G). The causal meaning of the large population remains unknown. Furthermore, Sirius red staining revealed more abundant fibrosis in both KO mouse TA muscles, a sign of disrupted regeneration, than in WT muscles (Figures 1H and 1I). These results uncovered opposing roles of Cry1 and Cry2: Cry1 as an inhibitor and Cry2 as a promoter of muscle regeneration. The increased fibrosis in *Cry1*$^{-/-}$ TA muscles is an exception to this conclusion; it is possible that *Cry1* KO does more than accelerate muscle regeneration.

Primary myoblasts were isolated from mice to investigate whether these muscle phenotypes were cell-autonomous. More than 98% of the cells of each mouse strain expressed MyoD, validating successful purification (Figures 2A and 2B). Even before induction of differentiation, the expression of sarcomeric MHC (a marker for differentiating myocytes) was higher in *Cry1*$^{-/-}$ myoblasts and lower in *Cry2*$^{-/-}$ myoblasts than in WT myoblasts (Figure 2B). Upon induction of differentiation with 5% horse serum (HS), MHC was expressed only in 43% of *Cry2*$^{-/-}$ myoblasts, in contrast with 63% in WT and 81% in *Cry1*$^{-/-}$ cells on day 1 (Figures 2A and 2C). Although MHC was activated in more than 95% of WT and *Cry1*$^{-/-}$ myoblasts by day 2, *Cry2*$^{-/-}$ myoblasts lagged behind (Figure 2D). We also calculated the fusion index in each cell type by dividing the

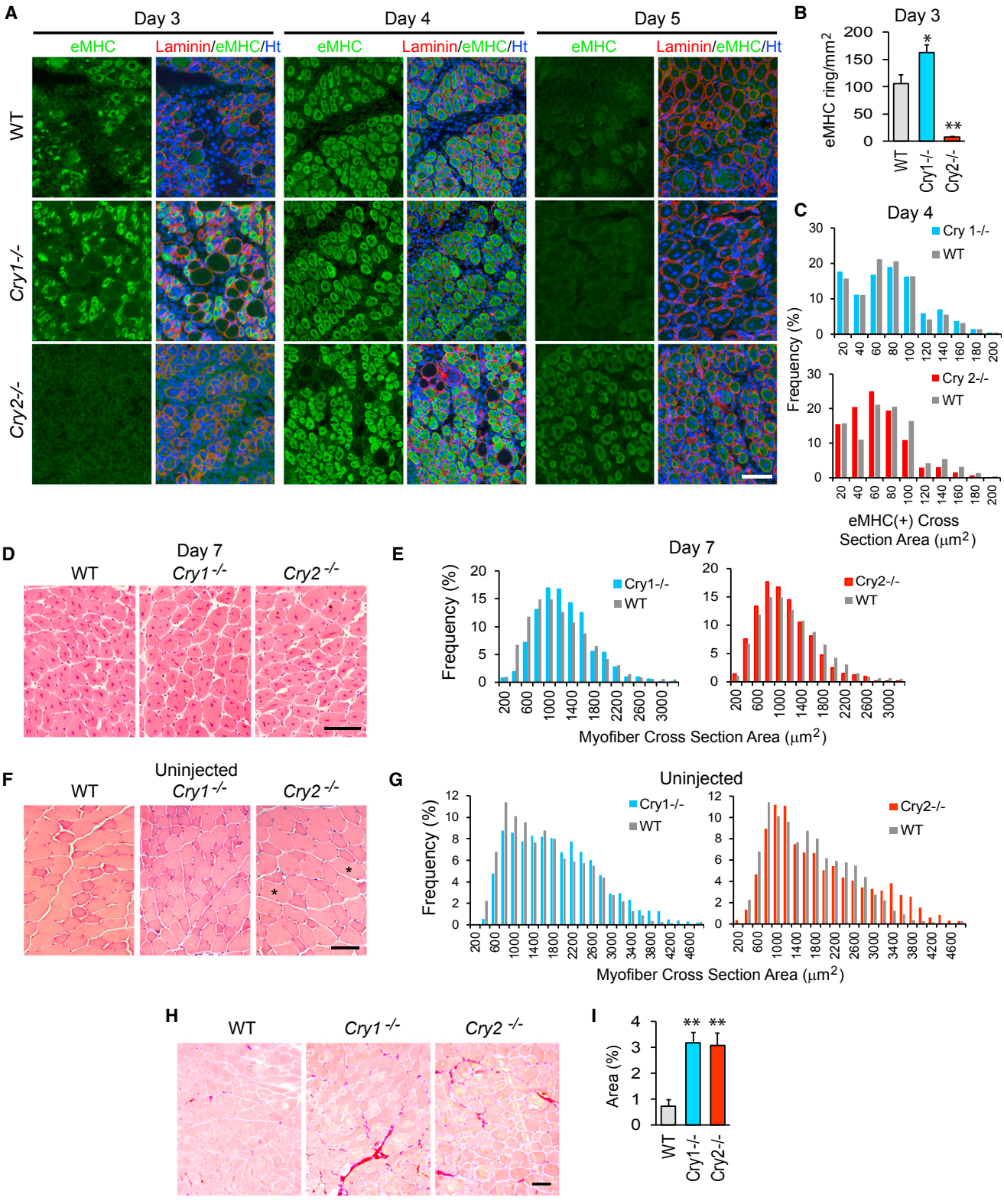

Figure 1. Regeneration of TA Muscle in *Cry1*$^{-/-}$ and *Cry2*$^{-/-}$ Mice

(A) Immunofluorescence staining of TA muscle with eMHC antibody on days 3, 4, and 5 after injection with barium chloride. Laminin staining defines the border of each myofiber. DNA was counterstained with Hoechst 33342. TA muscles were damaged and harvested between 10 a.m. and 2 p.m. (zeitgeber time 4 [ZT4] and

(legend continued on next page)

number of nuclei located within MHC(+) cells containing two or more nuclei by the total number of nuclei in a given field. The fusion index was higher in *Cry1*$^{-/-}$ myoblasts and lower in *Cry2*$^{-/-}$ myoblasts compared with WT myoblasts on differentiation day 3 (Figure 2E). The differences in fusion efficiency were also highlighted by the < 3 nuclei index, which was obtained by dividing the number of nuclei residing in MHC(+) cells that contained only one or two nuclei by the number of nuclei in all MHC(+) cells. The index was lower in *Cry1*$^{-/-}$ myoblasts and higher in *Cry2*$^{-/-}$ myoblasts compared with the WT (Figure 2F). Furthermore, after single muscle fibers were isolated and cultured for 72 hr, the frequency MyoD(+)Pax7(−) differentiating myoblasts were higher with *Cry1*$^{-/-}$ fibers and lower with *Cry2*$^{-/-}$ fibers compared with WT fibers (Figures S1A and S1B). Thus, myogenic differentiation was cell-autonomously promoted in *Cry1*$^{-/-}$ myoblasts but inhibited in *Cry2*$^{-/-}$ myoblasts *in vitro*, recapitulating *in vivo* muscle regeneration.

Cry1 KD Promotes but *Cry2* KD Inhibits Myoblast Differentiation *In Vitro*

To understand the molecular mechanisms underlying the differential effects of *Cry1* and *Cry2* KO, we differentiated mouse myoblast C2C12 cells as a model after KD of the *Cry1* and *Cry2* genes. Two shRNA clones decreased each target mRNA level to lower than 20% of scrambled control short hairpin RNA (shRNA) (Figure S1C). The KD cells were induced for myogenic differentiation and stained with an MHC antibody. On days 3 and 5 of differentiation, MHC(+) cells were more dense with *Cry1* KD but more sparse and shorter with *Cry2* KD than the control (Figure 3A). Consistently, the differentiation index, defined as the frequency of nuclei existing in MHC(+) cells among all nuclei, was higher in *Cry1* KD cells and lower in *Cry2* KD cells than in control cells on day 5 (Figure 3B). A similar trend in the expression of MHC was observed at the mRNA level on day 5 (Figure 3C). Additionally, *Cry1* KD upregulated three other markers for differentiation: myogenin, myomaker, and creatine kinase M (Ckm), compared with the control. The lower fusion index and the higher < 3 nuclei index in *Cry2* KD cells (Figures 3D and 3E) suggested that impaired cell fusion was an underlying mechanism for the short myotube phenotype. Overall, the KD experiments with C2C12 cells recapitulated the phenotypes observed with the primary myoblasts isolated from the KO mice.

The total number of nuclei in *Cry2* KD cells was less than 80% of control cells on differentiation day 5 (Figure 3F). *Cry2* KD promoted cell cycle exit during differentiation, as shown by the more rapid decline of the uptake of 5-ethynyl-2′-deoxyuridine (EdU) compared with the control and *Cry1* KD cells (Figure 3G). However, before differentiation induction, all cell types proliferated at similar rates, as shown with an MTS assay ([3-(4,5-dimethylthiazol-2-yl)-5-(3-carboxymethoxyphenyl)-2-(4-sulfophenyl)-2H-tetrazolium, inner salt]) (Figure S1D). The lower cell density in the *Cry2* KD wells could be a reason for the inefficient cell fusion and the consequent short myotube phenotype; however, the differentiation index and fusion index remained lower and the < 3 nuclei index was higher compared with control cells when 50% more cells were seeded before differentiation (Figures S1E–S1G). These results indicate that inefficient cell fusion with the *Cry2* KD was not due to early exit from the cell cycle.

Differential Gene Expression by *Cry1* and *Cry2* KD

We compared RNA sequencing (RNA-seq) data between each KD and control cell line on differentiation days 0, 3, and 5 to understand the mechanisms underlying the opposing roles of Cry1 and Cry2 in myogenic differentiation (Figures S2A). Genes that were expressed at > 200% or < 50% of the control level were selected for further analyses. More genes were differentially expressed between each KD compared with the number of genes that were up or downregulated in both KDs (Figure 4A). Gene ontology (GO) analysis of the differentially expressed genes indicated that muscle-specific genes, including those indicative of differentiation (myogenin, myomaker [also called Tmem8c], MHC 1 and 3, and myosin light chain 1), were upregulated in *Cry1* KD cells compared with control and *Cry2* KD cells on day 0 (Figures S2B and S2C, highlighted in yellow). This suggested premature initiation of differentiation of *Cry1* KD cells; however, the difference disappeared on days 3 and 5. There was no GO term that could readily explain the delayed differentiation of *Cry2* KD cells.

ZT8), when *Cry1* and *Cry2* mRNA levels were low (Figure 4C). This was because the peak timing of these mRNA levels was variable among WT, *Cry1*$^{-/-}$, and *Cry2*$^{-/-}$ mice, leaving the lower expression level timing more consistent.

(B) The frequency of myofibers with eMHC staining in a ring shape in regenerating myofibers, identified by ring-shaped laminin staining on day 3. In undamaged myofibers, eMHC was not expressed, and laminin staining displayed polygonal shapes. eMHC staining was defined as a ring shape with an unstained area in the center, corresponding to a centrally located nucleus, with a diameter larger than 10 μm. Muscle areas of 5 mm^2 were observed in each mouse, and two mice were used for each strain.

(C) Size distribution of eMHC(+) myofiber cross-sections on day 4. We measured 2,000 myofibers from two mice, totaling 4,000 myofibers for each strain. Chi-square analysis indicates that *Cry1*$^{-/-}$ myofibers were larger and that *Cry2*$^{-/-}$ myofibers were smaller than those of the WT, with $p < 0.01$. Average sizes of myofiber cross-section areas are as follows: WT, 66.2 μm^2; *Cry1*$^{-/-}$ 68.4 μm^2; and *Cry2*$^{-/-}$ 55.7 μm^2.

(D) H&E staining of day 7 TA sections.

(E) Size distribution of the H&E-stained myofiber cross-sections on day 7. 500 randomly selected myofibers from four mice, totaling 2,000 myofibers for each mouse strain, were measured. Chi-square analysis indicates that *Cry1*$^{-/-}$ myofibers were larger and that *Cry2*$^{-/-}$ myofibers were smaller than WT myofibers, with $p < 0.01$. Average sizes of myofiber cross-section areas are as follows: WT, 1,111.7 μm^2; *Cry1*$^{-/-}$ 1,136.4 μm^2; and *Cry2*$^{-/-}$, 1,018.2 μm^2.

(F) H&E staining of uninjected TA sections. Unusually large myofibers are marked with asterisks.

(G) Size distribution of the cross-sections of uninjected myofibers. Two thousand myofibers for each mouse strain were measured as described in (E). *Cry1*$^{-/-}$ myofibers were larger than WT myofibers, with $p < 0.01$ from Chi-square analysis. Average sizes of myofibers are as follows: WT, 1,580.4 μm^2; *Cry1*$^{-/-}$, 1,815.0 μm^2; and *Cry2*$^{-/-}$, 1,789.6 μm^2.

(H) Sirius red staining of uninjected TA muscles isolated from 10-week-old mice.

(I) Area percentage of fibrosis, indicated by positive Sirius red staining in (H).

*$p < 0.05$ and **$p < 0.01$ with Student's t test. Data are presented as mean + SD in (B) and (I). Scale bars, 100 μm.

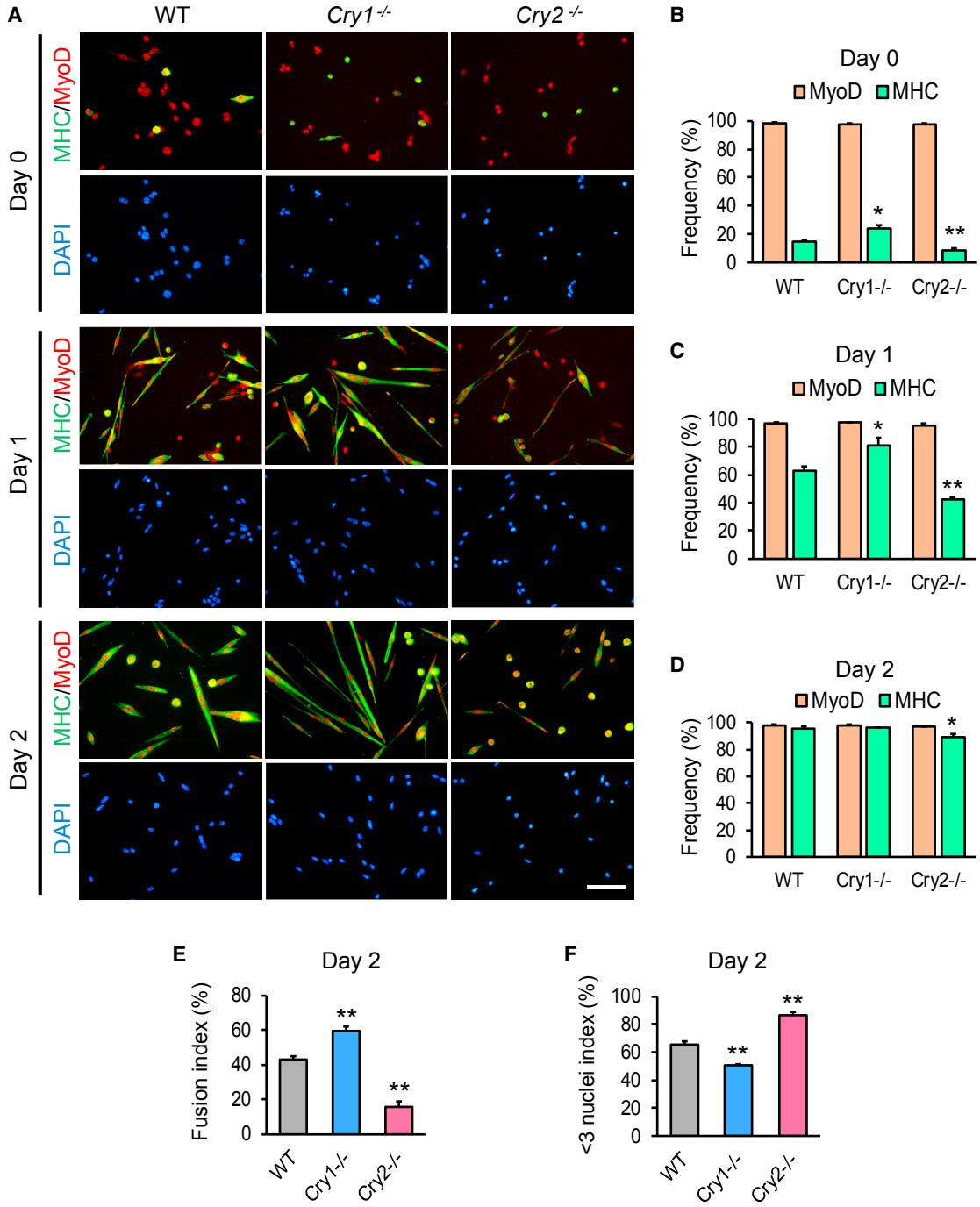

Figure 2. Differentiation of *Cry1*$^{-/-}$ and *Cry2*$^{-/-}$ Myoblasts

(A) Immunostaining of primary myoblasts prepared from WT, *Cry1*$^{-/-}$, and *Cry2*$^{-/-}$ mice with antibodies against MHC and MyoD. Cells were induced to differentiate with 5% HS for 1 and 3 days. Scale bar, 50 μm.

(B–D) Frequency of nuclei within MyoD(+) or MHC(+) cells among 500 total nuclei on day 0 (B), day 1 (C), and day 2 (D).

(E and F) Fusion index (E) and < 3 nuclei index (F) on day 2, based on observation of 500 nuclei.

Data are presented as mean + SD.

However, further inspection of the RNA-seq data revealed that the expression level of *Ccnd1* (cyclin D1) was lower in *Cry2* KD cells than in the control and *Cry1* KD cells on day 3 (Figure S2D, arrow). In contrast, *Ccnd2* (cyclin D2) was not lower in *Cry2* KD cells compared with the other cells (Figures S2D and S2E). qPCR verified prominent downregulation of *Ccnd1* in *Cry2* KD

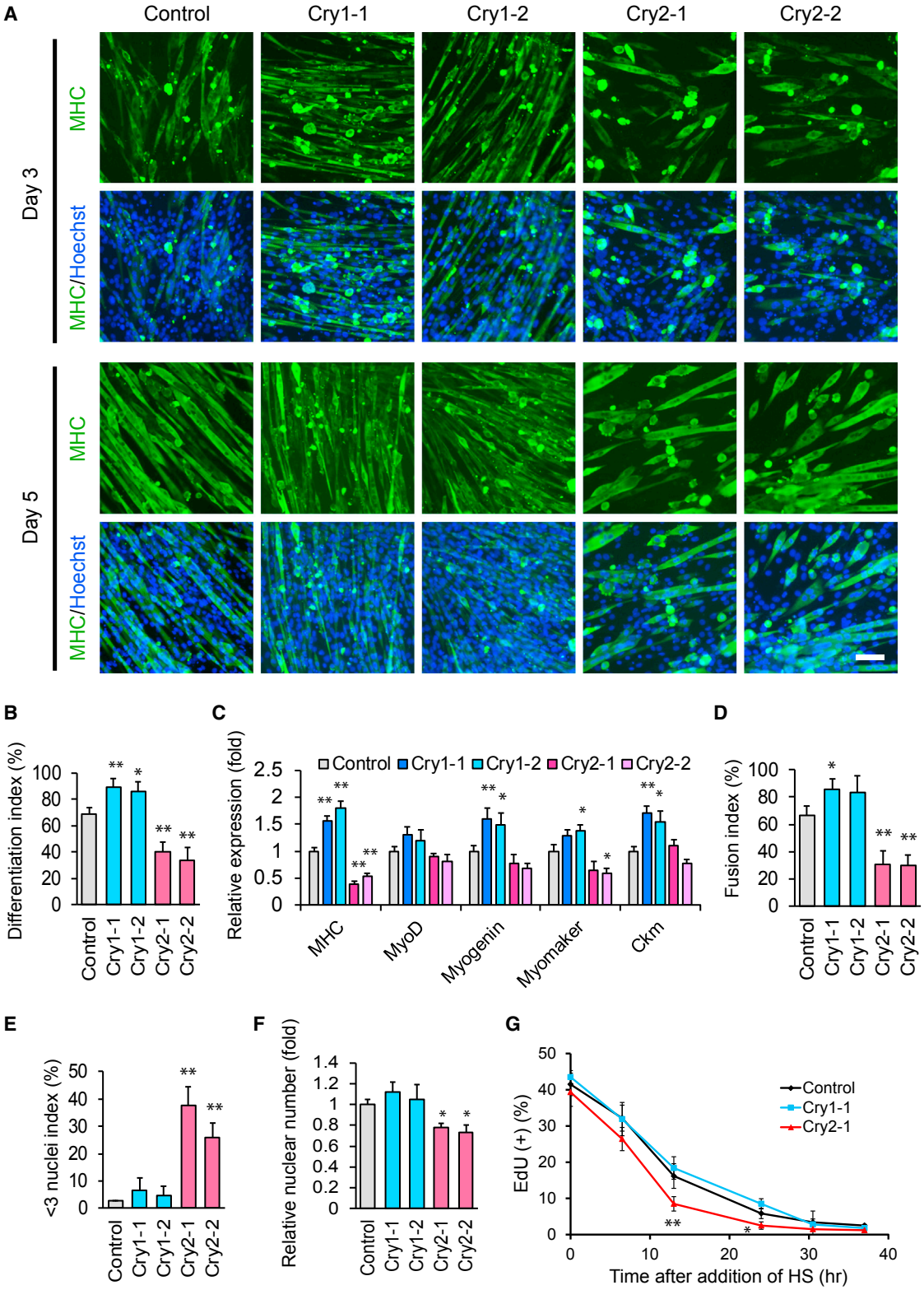

Figure 3. Differentiation of C2C12 Cells after KD of *Cry1* and *Cry2*

(A) MHC staining of C2C12 KD cells during differentiation. Two shRNA clones each were used for *Cry1* and *Cry2* KD. Scale bar, 100 μm.

(B) Differentiation index on day 5, obtained from the observation of 1,000 nuclei.

(legend continued on next page)

cell lines established with two shRNA clones on days 1, 3, and 5 (Figure 4B). *Ccnd1* is known to be downregulated upon initiation of myoblast differentiation, which leads to cell cycle exit (Walsh and Perlman, 1997). The premature downregulation of *Ccnd1* in *Cry2* KD cells could potentially explain the early cell cycle exit of *Cry2* KD cells, as studied below.

Early Cell Cycle Exit in *Cry2* KD Cells because of the Downregulation of Cyclin D1

Ccnd1 expression is regulated by circadian rhythms in the liver (Feillet et al., 2015; Soták et al., 2014), but the Cry2-specific contribution to *Ccnd1* expression has not been reported. To understand whether Cry2 regulates the circadian expression pattern of *Ccnd1 in vivo*, the mRNA levels of circadian regulators and *Ccnd1* in TA muscle were determined with qPCR every 4 hr for 44 hr. Consistent with a previous work (Andrews et al., 2010) and the Circadian Expression Profiles Database (CircaDB; http://circadb.hogeneschlab.org/), *Bmal1*, *Per1*, *Cry1*, and *Cry2* were expressed in TA muscle in circadian manners, although there was variation in the peak timing of the same genes between each strain (Figure 4C). *Cry1* and *Cry2* were not upregulated in $Cry2^{-/-}$ TA muscle and $Cry1^{-/-}$ TA muscle, respectively, indicating a lack of compensatory upregulation between the two genes. Importantly, although *Ccnd1* also showed circadian expression patterns in WT and $Cry1^{-/-}$ TA muscle, the amplitude of the oscillation was substantially weakened in $Cry2^{-/-}$ TA muscle, indicating Cry2-dependent circadian oscillation of the *Ccnd1* mRNA level in TA muscle.

Because TA muscle is a mixture of mitotically quiescent myofibers and many other types of proliferating cells, we turned to C2C12 cells to separately characterize the expression in proliferating C2C12 myoblasts and differentiating C2C12 cells that were undergoing cell cycle exit. In the first experiment with undifferentiated C2C12 cells, the circadian rhythms of the sparsely seeded cells were synchronized with forskolin between −1 and 0 hr, and the cells were harvested every 4 hr thereafter while they were proliferating. *Cry1* and *Cry2* levels showed typical circadian rhythms with around a 24-hr period in control cells, whereas their levels were consistently low in each KD cell line, verifying effective KD throughout the experiments (Figure 4D). The *Ccnd1* level and EdU uptake also demonstrated circadian oscillation in all three cell types with similar amplitudes (Figures 4D and 4E). The lack of *Ccnd1* downregulation in *Cry2* KD cells agreed with the PCR result of non-synchronized day 0 cells (Figure 4B).

In the second experiment, circadian rhythms in confluent C2C12 cells were synchronized with forskolin between −1 and 0 hr, and differentiation was induced at 0 hr. *Cry1* and *Cry2* were expressed in a circadian manner during differentiation for 120 hr in control and *Cry1* KD cells (Figure 4F). *Ccnd1* levels gradually decreased, with several transient upregulation peaks in these cells. However, the intermittent peaks were not observed with *Cry2* KD cells. Consistently, the circadian pattern of EdU uptake seen in the control and *Cry1* KD cells disappeared in *Cry2* KD cells (Figure 4G). The numbers of total nuclei at 120 hr of differentiation were substantially lower in *Cry2* KD cells compared with control cells, reflecting the lost EdU uptake peaks (Figure 4H). Together, these results demonstrate that *Ccnd1* mRNA was expressed in a circadian manner in both undifferentiated and differentiating cells and that its downregulation by *Cry2* KD became prominent only during differentiation.

Although previous results showed that a lower cell number was not the cause for the inefficient cell fusion in *Cry2* KD cells, we verified this point with *Ccnd1* KD cells. After KD of *Ccnd1* with two shRNAs (Figure S3A), cells were induced to differentiate (Figure S3B). Nuclear numbers on day 5 were lower with the KD cells than with control cells, as expected (Figure S3C). We did not find statistically significant differences in differentiation index, fusion index, or < 3 index between control and *Ccnd1* KD cells (Figures S3D–S3F). Thus, downregulation of *Ccnd1* by *Cry2* KD cannot explain the inefficient cell fusion with the KD cells.

Inefficient Cell Fusion in *Cry2* KD Cells because of the Lack of Tmem176b

We searched for additional candidate genes within the RNA-seq data to explain the inefficient cell fusion by *Cry2* KD. This identified the transmembrane protein gene *Tmem176b* as a promising candidate. First, its expression level was lower throughout differentiation in non-synchronized *Cry2* KD cells than in other cells, according to RNA-seq (Figure S4A, arrows) and qPCR (Figure 5A). The expression level of *Tmem176b* showed circadian oscillation in TA muscle in WT and $Cry1^{-/-}$ mice as well as in differentiating C2C12 cells after synchronization of the control and *Cry1* KD cells (Figures 5B and 5C). However, the expression was downregulated with weakened circadian oscillation in *Cry2* KO TA muscle and KD cells. CircaDB also indicates that *Tmem176b* shows a circadian expression pattern in skeletal muscle. In addition, Tmem176b shares 67.4% similarity at the amino acid level with myomaker, one of the best characterized fusion inducers (Millay et al., 2013).

To examine whether Tmem176b is involved in myogenic differentiation, its KD cells were induced to differentiate (Figures S4B and 5D). *Tmem176b* KD cells showed lower differentiation indexes (Figure 5E); the fusion indexes were also lower, and the < 3 nuclei indexes were markedly increased by the KD (Figures 5F and 5G). Next, the circadian pattern of myogenic cell fusion in synchronized cells was assessed by categorizing the cells based on the number of nuclei within MHC(+) myocytes/myotubes. In control cells, the percentage of nuclei in MHC(+) cells containing only one nucleus suddenly decreased, whereas the percentage of nuclei in MHC(+) cells containing two nuclei increased sharply between 64 to 68 hr (Figure 5H, control, **).

(C) Relative expression levels of five muscle genes determined by qPCR on day 5. The value obtained with control cells was defined as 1.0.
(D and E) Fusion index (D) and < 3 nuclei index (E) of KD cells on day 5, obtained from the observation of 1,000 nuclei.
(F) Relative nuclear number of KD cells on day 5. The number of control nuclei was defined as 1.0. The results were calculated by counting nuclei in four different fields with a 20× lens.
(G) Temporal profile of the frequency of EdU(+) nuclei in KD cells after induction of differentiation. The results were obtained by counting 1,000 nuclei.
Data are presented as mean + or ± SD.

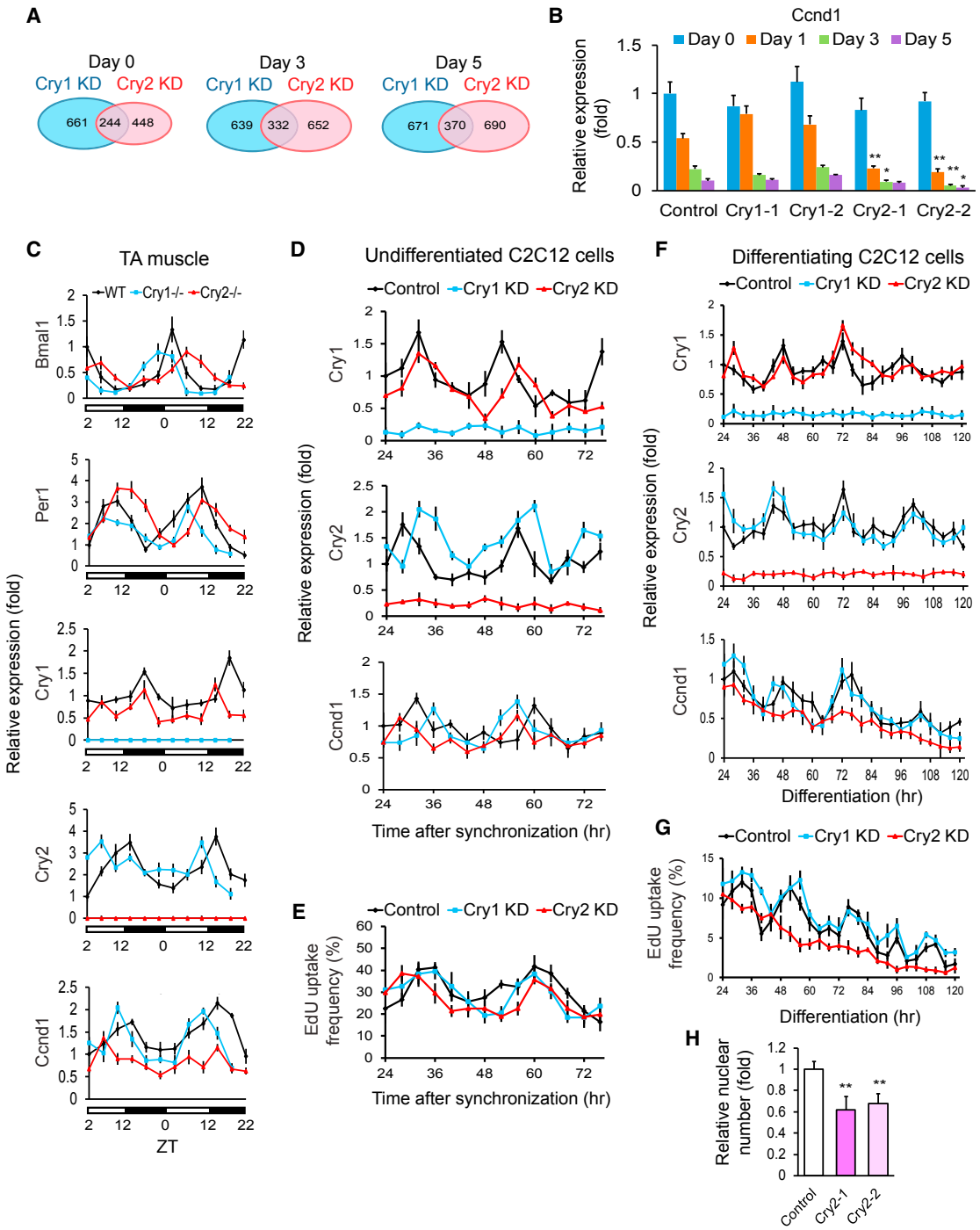

Figure 4. Gene Expression Analyses of KD C2C12 Cells

(A) Venn diagrams displaying the number of genes whose expression levels were > 200% or < 50% of those of control cells. shRNA clone 1 was used for *Cry1* and *Cry2* KD.

(B) qPCR results comparing the expression levels of *Ccnd1* during differentiation of KD cells. The value obtained with the control on day 0 was defined as 1.0.

(C) Temporal profiles of the indicated gene levels in the TA muscles of KO mice. WT expression values at ZT2 on the first day in the graph were defined as 1.0. The light was on between ZT0 and ZT12.

(D) Temporal profiles of indicated gene levels in undifferentiated KD cells after synchronization with forskolin between −1 and 0 hr. The control value at 24 hr was defined as 1.0. shRNA clone 1 was used for *Cry1* and *Cry2* KD. Cell harvest was initiated 24 hr after forskolin treatment to wait for recovery from its acute effects.

(E) Temporal profile of EdU uptake in undifferentiated and synchronized C2C12 cells. The results were obtained by counting 1,000 nuclei.

(legend continued on next page)

This was followed by a drastic increase of those in MHC(+) cells containing more than 10 nuclei between 84 and 88 hr and between 108 and 112 hr. *Cry1* KD cells showed a similar pattern between 88 and 92 hr and between 108 and 112 hr. In contrast, these sudden increases of fused cells were not observed with *Cry2* KD or *Tmem176b* KD cells. These results strongly indicate that downregulation of *Tmem176b* by *Cry2* KD indeed prevented proper cell fusion during differentiation. As a side note, *Cry1* KD increased the frequency of nuclei in MHC(+) cells containing 3–5 nuclei compared with control cells (Figure 5H, *Cry1* KD, green line), suggesting accelerated cell fusion. In a complementary study, overexpressed *Tmem176b* decreased the fusion index, but it was largely due to the lower differentiation index compared with control cells, as indicated by the similar values of the < 3 nuclei index between control and overexpressing cells (Figures S4C–S4G).

Identification of Bclaf1 as a Cry2-Specific Binding Protein

To understand how mRNA levels of *Ccnd1* and *Tmem176b* were regulated specifically by Cry2, Cry1- and Cry2-binding proteins were immunoprecipitated after overexpression of each FLAG-tagged protein in undifferentiated C2C12 cells (Figure 6A). We detected three peptide fragments of Bclaf1 (Bcl-2 associated factor 1) specifically in the co-precipitated protein pool with Cry2 in addition to three circadian regulators: Per1, Fbxl3 (F-box type E3 ligase for Cry proteins), and CK1δ (phosphorylates Per proteins) (Hirano et al., 2016) by high-resolution peptide tandem mass spectrometry and database searching after proteolytic digestion (Figures S5A and S5B). Cry2-specific interaction of Bclaf1 was verified by western blotting in the same immunoprecipitated protein pool (Figure 6B). Reciprocal immunoprecipitation of endogenous proteins also confirmed the interaction on day 3 differentiating cells (Figure 6C). *Bclaf1* is under circadian regulation in muscle (Andrews et al., 2010), TA muscle (Figure 6D, black line), and differentiating synchronized C2C12 cells (Figure 6E, black line). The *Bclaf1* circadian rhythms were not disrupted by KO or KD of *Cry2* (Figures 6D and 6E, red lines). Importantly, KD of *Bclaf1* (Figure S5D) decreased the circadian expression of *Ccnd1* and abolished the circadian uptake of EdU during differentiation (Figures 6F and 6G). Consistently, the nuclear numbers were substantially lower with *Bclaf1* KD cells on day 5 (Figure 6H). However, *Bclaf1* KD did not decrease the proliferation of the cells before induction of differentiation, which was similar to *Cry2* KD (Figure S5E). As for cell fusion, *Bclaf1* KD cells lost the circadian expression pattern of *Tmem176b* (Figure 6I) and showed lower differentiation indexes and fusion indexes and higher < 3 nuclei indexes than control cells (Figures 6J–6M). In summary, *Bclaf1* KD recapitulated two phenotypes of *Cry2* KD, promoted cell cycle exit and inefficient cell fusion, indicating that Bclaf1 cooperatively functions with Cry2 in *Ccnd1* and *Tmem176b* gene regulation.

Bclaf1 Regulates the Stability of *Ccnd1* and *Tmem176b* mRNAs

Previous work reported that Bclaf1 forms a protein complex that binds to and stabilizes *Ccnd1* mRNA, but not *Ccnd2*, in an osteosarcoma cell line (Bracken et al., 2008). We tested whether *Tmem176b* mRNA co-precipitates with Bclaf1 after immunoprecipitation of Bclaf1 (Figure 7A) from differentiation day 3 cells without shRNA. Indeed, *Ccnd1* and *Tmem176b* mRNAs were enriched in the precipitated RNA pool compared with two control genes: glyceraldehyde 3-phosphate dehydrogenase (*Gapdh*) and β-actin (*Actb*) (Figure 7B). mRNA stability was then assessed by quantifying mRNA levels while new transcription was inhibited by actinomycin D in undifferentiated KD cells. *Ctla2a* mRNA, whose half-life is 687 min in C2C12 cells (Lee et al., 2010), was used as a stable control mRNA (Figure S6A). *Bclaf1* KD substantially decreased the half-life of *Tmem176b* (control versus KD = 8.5 hr versus 2.3–4.1 hr) and *Ccnd1* mRNAs (9.1 hr versus 3.6 hr) but not *Ccnd2* mRNA (Figure 7C). Similarly, *Cry2* KD shortened the half-life of only *Tmem176b* and *Ccnd1* mRNAs (Figure 7D). This finding agrees with decreased binding of the mRNAs to Bclaf1 in *Cry2* KD cells (Figure 7E). In contrast, *Cry1* KD did not affect mRNA binding or mRNA stability (Figures S6B–S6D).

The levels of nascent mRNAs encoding *Ccnd1*, *Ccnd2*, and *Tmem176b* were not decreased by KD of *Bclaf1*, *Cry1*, or *Cry2* (Figure S7A), indicating that mRNA stability, rather than transcription, was disrupted by *Bclaf1* and *Cry2* KD. In addition, *Cry1* KD did not rescue the *Bclaf1* KD phenotypes (Figure S7B–S7F), which demonstrates that Cry1's promoted myoblast differentiation was independent of Bclaf1. This is in line with the results showing that *Cry1/2* double KD phenocopied *Cry2* KD (Figure S7G–S7K). Taken together, the cooperative stabilization of *Ccnd1* and *Tmem176b* mRNAs by Cry2 and Bclaf1 provides a mechanistic explanation for the significance of Bclaf1 in promoting circadian myoblast proliferation and myogenic fusion.

DISCUSSION

This study uncovered circadian regulation of myogenic differentiation through mRNA stabilization. The following working model summarizes our findings. In undifferentiated and proliferating myoblasts, *Ccnd1* is abundantly expressed, and its downregulation by instability because of the depletion of the Cry2-Bclaf1 complex is not evident, which allows cells to sustain a normal proliferation level. However, when differentiation begins and *Ccnd1* is transcriptionally downregulated, instability of the mRNAs by Cry2-Bclaf1 depletion becomes prominent, resulting in accelerated cell cycle exit. As for cell fusion, *Tmem176b* is continuously expressed regardless of the differentiation status; it is necessary to promote cell fusion when differentiation is initiated. Collectively, the coordinated circadian oscillation of

(F) Temporal profiles of the indicated gene levels in differentiating KD cells after synchronization with forskolin between −1 and 0 hr. The control value at 24 hr was defined as 1.0 for each gene.
(G) Temporal profile of EdU uptake during differentiation of synchronized KD cells.
(H) Relative nuclear number of KD cells 120 hr after differentiation. The number in control cells was defined as 1.0.
Data are presented as mean + or ± SD.

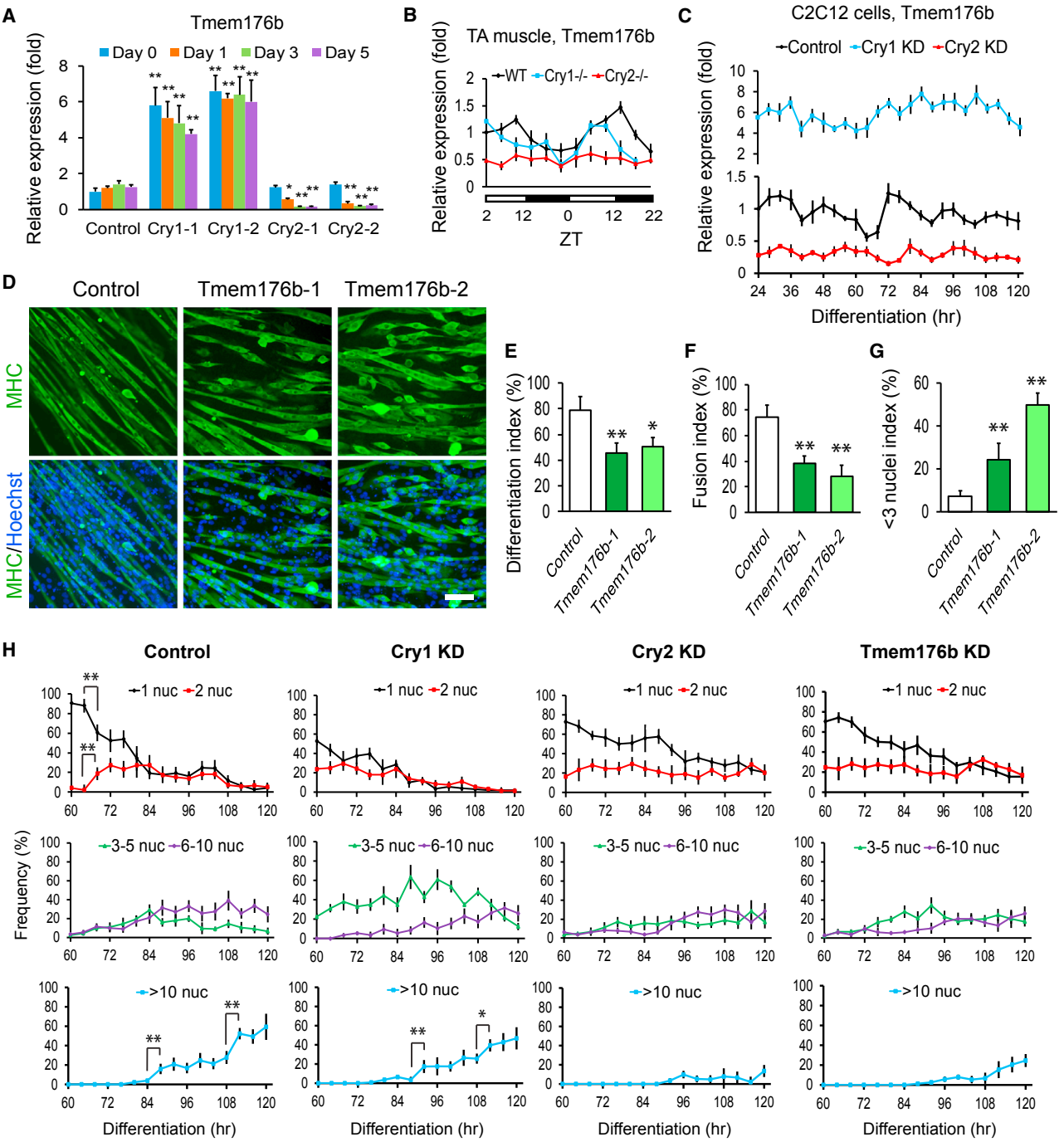

Figure 5. Inhibition of Cell Fusion with *Tmem176b* KD in C2C12 Cells

(A) qPCR comparing the expression levels of *Tmem176b* during differentiation of *Cry1* and *Cry2* KD cells. Two shRNA clones were used for each gene. The expression level of *Tmem176b* in day 0 control cells was defined as 1.0.

(B) Temporal profiles of *Tmem176b* expression levels in WT, *Cry1*$^{-/-}$, and *Cry2*$^{-/-}$ TA muscles.

(C) Temporal profiles of *Tmem176b* expression levels in C2C12 cells synchronized with forskolin between −1 and 0 hr and induced to differentiate at 0 hr. shRNA clone 1 was used for Cry1 and Cry2 KD.

(D) MHC staining of *Tmem176b* KD cells on differentiation day 5. Scale bar, 100 μm.

(E–G) Differentiation index (E), fusion index (F), and < 3 nuclei index (G) of *Tmem176b* KD cells on day 5.

(H) Frequency of nuclei in MHC(+) cells containing 1, 2, 3–5, 6–10, and more than 10 nuclei within one cell during differentiation. A total of 1,000 nuclei were counted at each time point.

Data are presented as mean + or ± SD.

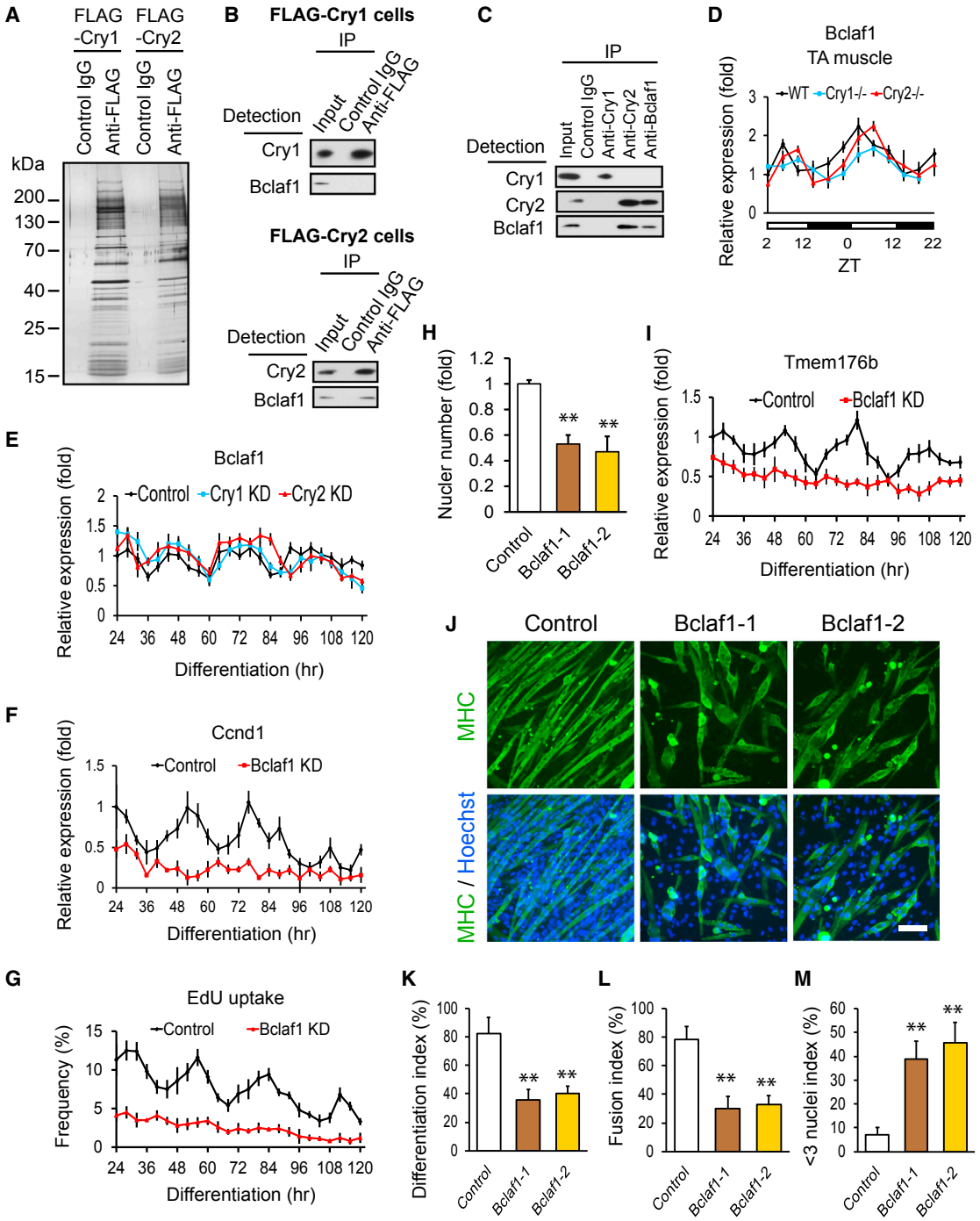

Figure 6. Regulation of *Ccnd1* and *Tmem176b* by Bclaf1

(A) Silver staining of a gel loaded with immunoprecipitated proteins from FLAG-Cry1- and FLAG-Cry2-expressing undifferentiated cells using an anti-FLAG antibody.

(B) Western blotting of immunoprecipitated proteins with an anti-FLAG antibody from FLAG-Cry1-expressing (top) and FLAG-Cry2-expressing (bottom) cells. Proteins were detected by the indicated antibodies.

(C) Western blotting of immunoprecipitated endogenous proteins with anti-Cry1, anti-Cry2, and anti-Bclaf1 antibodies from differentiation day 3 cells.

(D) Temporal profile of *Bclaf1* expression levels in TA muscles.

(E–G) Temporal profiles of expression levels of *Bclaf1* (E) and *Ccnd1* (F) and uptake of EdU (G) in KD cells during differentiation. shRNA clone 1 was used for *Cry1*, *Cry2*, and *Bclaf1* KD cells.

(H) Nuclear number in *Bclaf1* KD cells on day 5.

(legend continued on next page)

the expression levels of *Cry2*, *Bclaf1*, *Ccnd1*, and *Tmem176b* leads to circadian myoblasts proliferation and cell fusion during differentiation. However, it remains unknown whether there is any advantage for the circadian regulation of these processes. Another important question would be whether embryonic myoblast differentiation is also regulated by circadian rhythms. Unlike adult muscle regeneration, embryonic muscle differentiation takes place as a highly coordinated series of events in a spatial and temporal manner. Nonetheless, it is possible that maternal hormones and metabolism regulated by circadian rhythms add another layer to the regulation of the cell cycle and other events in embryonic development, including myogenesis.

In other model systems, circadian rhythms regulate gene activity at various post-transcriptional levels, including alternative splicing, polyadenylation, and mRNA nuclear export (Beckwith and Yanovsky, 2014; Preußner and Heyd, 2016). Such post-transcriptional regulation appears to be highly prevalent in circadian genes. A recent nascent RNA sequencing (nascent-seq) study showed that 70% of oscillating mRNAs in the liver demonstrate poor oscillation at the transcriptional level (Menet et al., 2012). However, previous works on the circadian regulation of myogenesis were primarily concerned with transcriptional activation of *MyoD* by Clock/Bmal1 (Andrews et al., 2010; Chatterjee et al., 2013; Lefta et al., 2011). Because Crys are supposed to inhibit Clock/Bmal1, they are expected to delay myogenesis, which Cry1 appears to achieve. In contrast, Cry2 plays an opposite role through post-transcriptional regulation. In this sense, Cry1 can be regarded as "classic" Cry, whereas Cry2 would be "deviated" Cry. The *Drosophila* genome encodes only one *cry* gene, which shares around 75% similarity with both mouse Crys at the amino acid level. Functional and structural comparison between mouse and *Drosophila* Crys could shed further light on the division of labor between mouse Cry1 and Cry2.

Another way to dissect the structural mechanism underlying the Cry2-specific interaction with Bclaf1 would be to create hybrid proteins between Cry1 and Cry2 as reported by Khan et al. (2012). They divided each protein into four domains and created a series of hybrid proteins swapping each domain. From this work, they found that the helical domain in the middle of the protein is necessary for the Cry1-specific circadian rhythm regulation in fibroblasts. Combined with mutagenesis at the amino acid level and a 3D structural model, they identified several amino acids exposed to the surface that are critical for regulation. The same domain swapping was also used to determine the Cry2-specific interaction with nuclear hormone receptors (Kriebs et al., 2017).

Bclalf1 was originally identified as a pro-apoptotic binding partner of the adenovirus protein E1B 19K (Kasof et al., 1999; Sarras et al., 2010). Bclaf1 was later found to be widely expressed and to play additional roles, such as transcriptional regulation and mRNA stabilization. A majority of *Bclaf1*$^{-/-}$ mice die within 2 days after birth because of major defects in lung development (McPherson et al., 2009). Bclaf1 contains an arginine/serine (RS) domain that mediates protein-protein interactions and is typically detected in proteins involved in mRNA processing (Shepard and Hertel, 2009). In our study, individual KD of *Cry2* and *Bclaf1* both lead to destabilization of bound mRNAs. A similar cooperative stabilization of bound mRNAs by multiple protein subunits has been reported with another Bclaf1 complex called the SNIP1/SkIP-associated RNA-processing complex (Bracken et al., 2008). Among the five subunits in the complex, three subunits, including Bclaf1, are necessary to maintain the expression level of *Ccnd1*. Our mass spectrometry did not detect other protein components in the complex; this could be due to technical differences or a cell type difference.

Tmem176b belongs to the MS4A membrane protein family, which is characterized by four transmembrane domains (tetraspanin) and is involved in membrane signaling, such as calcium influx in B cells (Zuccolo et al., 2010). *Tmem176b* is ubiquitously expressed, but the most prominent phenotypes of *Tmem176b*$^{-/-}$ mice are disorganized cerebellar development and severe ataxia (Maeda et al., 2006). Currently, muscle abnormalities of *Tmem176b*$^{-/-}$ mice have not been reported. Tmem176b is distantly related to myomaker, which is essential for cell fusion (Millay et al., 2013). Unlike Tmem176b, myomaker contains seven transmembrane domains and does not belong to the MS4A family. However, Tmem176b and myomaker share 67.4% similarity within the 129 amino acids in the amino terminus of Tmem176b and the carboxyl terminus of myomaker, which contains a necessary region for its fusogenic function (Millay et al., 2016). Overexpression of Tmem176b did not promote cell fusion, which is similar to the result from the overexpression of myomaker (Millay et al., 2013). This could be because interacting proteins also need to be overexpressed to promote cell fusion, given the complex process of membrane fusion during myogenesis (Demonbreun et al., 2015; Kim et al., 2015). Additionally, the expression level of *Tmem176b* did not increase during differentiation in control C2C12 cells (Figure 5A). These results indicate that, although Tmem176b is necessary for efficient cell fusion, it is not a limiting factor that defines the pace of the fusion. In addition to inhibited cell fusion, *Tmem176b* KD decreased differentiation index (Figure 5E), suggesting that it is involved in additional differentiation programs, potentially through a membrane signaling mechanism. This possibility needs further study.

The differential roles between Cry1 and Cry2 suggest that Per1 and Per2 might also play distinct roles in myogenic differentiation. A chromatin immunoprecipitation sequencing (ChIP-seq) analysis indicated that the six core circadian regulators (Clock, Bmal1, Cry1/2, and Per1/2) have hundreds of chromatin binding sites unique to each of them, in addition to 1,444 common binding sites (Koike et al., 2012). The current approach of using synchronized myoblasts would provide a powerful *in vitro* model to investigate the unique functions of each regulator, which would, in turn, shed light onto mechanisms

(I) Temporal profiles of expression levels of *Tmem176b* in *Bclaf1* KD cells during differentiation.
(J) MHC staining of *Bclaf1* KD cells on day 5. Scale bar, 100 μm.
(K–M) Differentiation index (K), fusion index (L), and < 3 nuclei index (M) of *Bclaf1* KD cells on day 5.
Data are presented as mean + or ± SD.

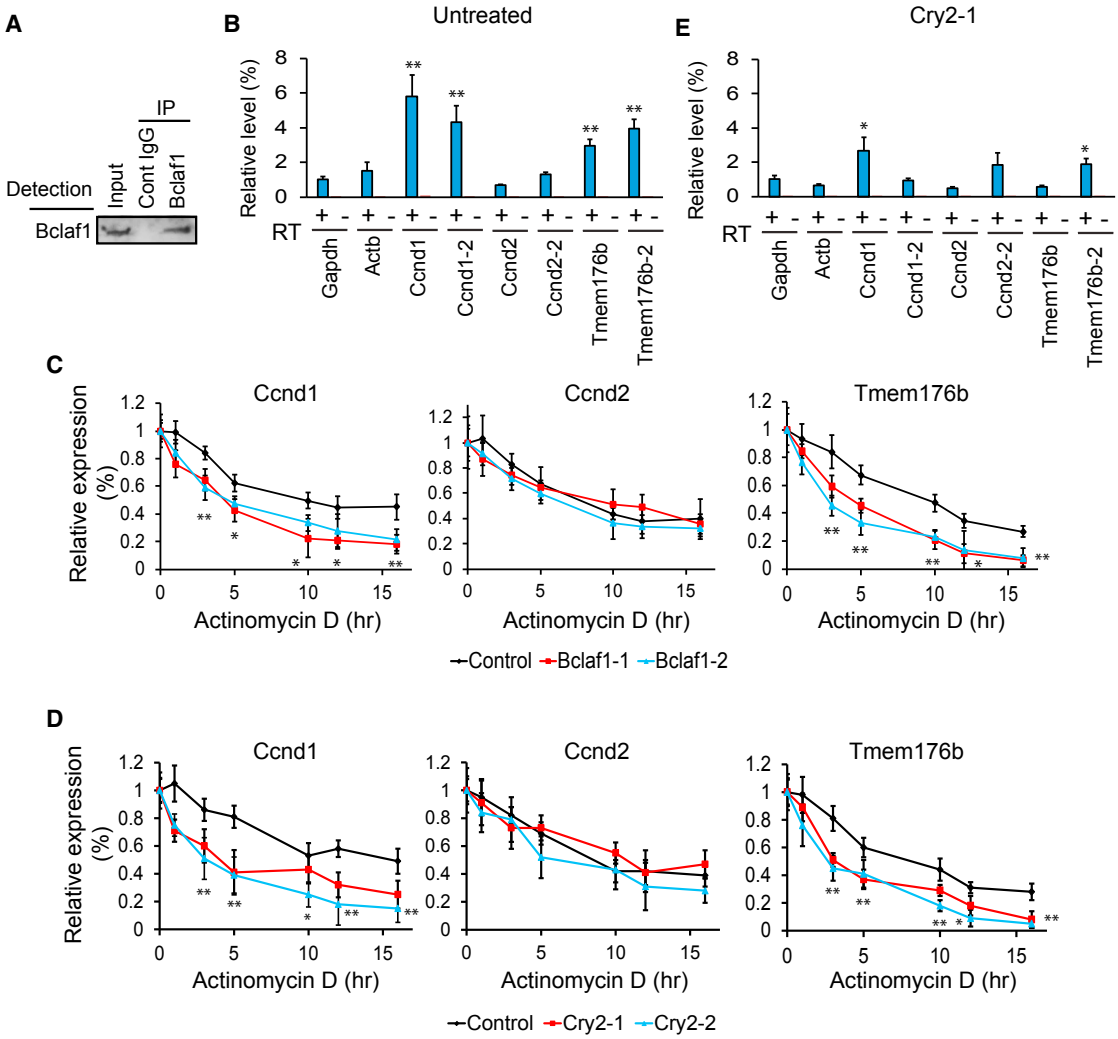

Figure 7. Stabilization of *Ccnd1* and *Tmem176b* mRNAs by Bclaf1

(A) Western blotting of immunoprecipitated Bclaf1 from differentiation day 3 cells.

(B) Relative expression levels of mRNAs in co-immunoprecipitated material with a Bclaf1 antibody. Results with and without reverse transcription are shown. Two PCR primer sets were used for *Ccnd1*, *Ccnd2*, and *Tmem176b*.

(C and D) Relative expression levels of three mRNAs in *Bclaf1* KD (C) and *Cry2* KD (D) cells treated with actinomycin D. The expression levels were normalized against *Ctla2a* mRNA at each time point and subsequently against 0 hr for each gene.

(E) Relative expression levels of mRNAs in co-immunoprecipitated material with a Bclaf1 antibody from *Cry2* KD cells on day 3.

Data are presented as mean + or ± SD.

underlying circadian rhythm-regulated myogenic differentiation and muscle regeneration.

EXPERIMENTAL PROCEDURES

KO Mice

All protocols were approved by the Institutional Animal Care and Usage Committee of the University of Minnesota (1602-33471A and 1604-33660A). *Cry1*$^{+/-}$ mice (B6.129P2-Cry1^{tm1Asn}/J, stock number 016186) and *Cry2*$^{+/-}$ mice (B6.129P2-Cry2^{tm1Asn}/J, stock number 016185) were purchased from Jackson Laboratory. Two to four mice of mixed genders at the age of 6 to 12 weeks were used unless specified otherwise. Age-matched littermate WT mice were used as controls. We injected 50 μL 1.2% $BaCl_2$ in 0.9% NaCl into the left TA muscle of four WT, *Cry1*$^{-/-}$, and *Cry2*$^{-/-}$ mice. Cryosections with a thickness of 10 μm were prepared for immunofluorescence, H&E, and Sirius red staining.

Circadian Gene Expression in TA Muscles

WT, *Cry1*$^{-/-}$, and *Cry2*$^{-/-}$ male mice were entrained at 12-hr light and 12-hr dark cycles (6 a.m. to 6 p.m. light and 6 p.m. to 6 a.m. dark) for 2 weeks before experiments. This means that zeitgeber time 0 (ZT0) corresponds to 6 a.m. and ZT12 to 6 p.m. TA muscles were isolated every 4 hr starting at ZT2.

Synchronization of Circadian Rhythms of Undifferentiated and Proliferating C2C12 Cells

C2C12 cells were seeded on day −1. On day 1, 10 μM forskolin was added between −1 and 0 hr. Cells were washed with PBS twice, and fresh 10% fetal bovine serum (FBS) in DMEM was added at 0 hr. Cells were harvested for PCR

or fixed for immunofluorescence staining every 4 hr for 44 hr. Cells were also pulse-labeled with 0.5 μM EdU for 30 min at each time point.

Synchronization of Circadian Rhythms of Differentiating C2C12 Cells

C2C12 cells were seeded on day −2. On day 0, forskolin was added between −1 and 0 hr. Cells were washed with PBS, and differentiation was started at 0 hr. Cells were harvested for PCR, fixed for immunofluorescence staining, or treated with EdU every 4 hr for 120 hr.

Statistical Analysis

Student's t test was used in the analysis of statistical significance of the difference in qRT-PCR data. The mean + SD obtained from three independent tests is shown in each graph. A chi-square test was used to determine the statistical significance of the difference in the histograms of muscle regeneration in Figure 1. The test was applied to the heart of the histogram, where the raw expected values were more than 5 cells per bin, with the WT as the expected value and the *Cry1*$^{-/-}$ or *Cry2*$^{-/-}$ as the actual values.

DATA AND SOFTWARE AVAILABILITY

The accession number for the RNA-seq data reported in this paper is GEO: GSE100898.

SUPPLEMENTAL INFORMATION

Supplemental Information includes Supplemental Experimental Procedures, seven figures, and two tables and can be found with this article online at https://doi.org/10.1016/j.celrep.2018.01.077.

ACKNOWLEDGMENTS

We acknowledge Minnesota Supercomputing Institute, University of Minnesota Informatics Institute, and University of Minnesota Genomics Center for providing high-performance computing resources and the gopher pipelines. We recognize the Center for Mass Spectrometry and Proteomics at the University of Minnesota and various supporting agencies, including the National Science Foundation for Major Research Instrumentation (grants 9871237 and NSF-DBI-0215759). Supporting agencies are listed at http://www.cbs.umn.edu/msp/about. A.Y. was supported by the Minnesota Stem Cell Institute. A.A. was supported by the NIH (R01 AR062142 and R21 AR070319). N.K was supported by the NIH (R01 GM098294, R21 AR066158, R21 HD083648, and R21 CA187232), the Engdahl Foundation, an Adjacent Possible Grant, and the University of Minnesota Foundation (4160-9227-13).

AUTHOR CONTRIBUTIONS

Conceptualization, A.A. and N.K.; Formal Analysis, C.Y.; Investigation, M. Lowe, J.L., E.P., D.M., R.H., C.Y., N.K.-K., M.R.-E., Y.A., J.S., M.Q., M. Lohman, A.A., and N.K.; Writing – Original Draft, A.A. and N.K.; Writing – Review & Editing, M. Lowe., E.P., D.M., M.R.-E., A.A., and N.K.; Supervision, A.A. and N.K.; Funding Acquisition, A.A. and N.K.

DECLARATION OF INTERESTS

The authors declare no competing interests.

Received: July 19, 2017
Revised: January 9, 2018
Accepted: January 25, 2018
Published: February 20, 2018

REFERENCES

Andrews, J.L., Zhang, X., McCarthy, J.J., McDearmon, E.L., Hornberger, T.A., Russell, B., Campbell, K.S., Arbogast, S., Reid, M.B., Walker, J.R., et al. (2010). CLOCK and BMAL1 regulate MyoD and are necessary for maintenance of skeletal muscle phenotype and function. Proc. Natl. Acad. Sci. USA *107*, 19090–19095.

Beckwith, E.J., and Yanovsky, M.J. (2014). Circadian regulation of gene expression: at the crossroads of transcriptional and post-transcriptional regulatory networks. Curr. Opin. Genet. Dev. *27*, 35–42.

Boucher, H., Vanneaux, V., Domet, T., Parouchev, A., and Larghero, J. (2016). Circadian clock genes modulate human bone marrow mesenchymal stem cell differentiation, migration and cell cycle. PLoS ONE *11*, e0146674.

Bracken, C.P., Wall, S.J., Barré, B., Panov, K.I., Ajuh, P.M., and Perkins, N.D. (2008). Regulation of cyclin D1 RNA stability by SNIP1. Cancer Res. *68*, 7621–7628.

Buchi, K.N., Moore, J.G., Hrushesky, W.J., Sothern, R.B., and Rubin, N.H. (1991). Circadian rhythm of cellular proliferation in the human rectal mucosa. Gastroenterology *101*, 410–415.

Buhr, E.D., and Takahashi, J.S. (2013). Molecular components of the Mammalian circadian clock. Handb. Exp. Pharmacol. *15*, 3–27.

Chatterjee, S., Nam, D., Guo, B., Kim, J.M., Winnier, G.E., Lee, J., Berdeaux, R., Yechoor, V.K., and Ma, K. (2013). Brain and muscle Arnt-like 1 is a key regulator of myogenesis. J. Cell Sci. *126*, 2213–2224.

Demonbreun, A.R., Biersmith, B.H., and McNally, E.M. (2015). Membrane fusion in muscle development and repair. Semin. Cell Dev. Biol. *45*, 48–56.

Feillet, C., van der Horst, G.T., Levi, F., Rand, D.A., and Delaunay, F. (2015). Coupling between the circadian clock and cell cycle oscillators: implication for healthy cells and malignant growth. Front. Neurol. *6*, 96.

Geyfman, M., Kumar, V., Liu, Q., Ruiz, R., Gordon, W., Espitia, F., Cam, E., Millar, S.E., Smyth, P., Ihler, A., et al. (2012). Brain and muscle Arnt-like protein-1 (BMAL1) controls circadian cell proliferation and susceptibility to UVB-induced DNA damage in the epidermis. Proc. Natl. Acad. Sci. USA *109*, 11758–11763.

Harfmann, B.D., Schroder, E.A., and Esser, K.A. (2015). Circadian rhythms, the molecular clock, and skeletal muscle. J. Biol. Rhythms *30*, 84–94.

Hirano, A., Fu, Y.H., and Ptáček, L.J. (2016). The intricate dance of post-translational modifications in the rhythm of life. Nat. Struct. Mol. Biol. *23*, 1053–1060.

Huber, A.L., Papp, S.J., Chan, A.B., Henriksson, E., Jordan, S.D., Kriebs, A., Nguyen, M., Wallace, M., Li, Z., Metallo, C.M., and Lamia, K.A. (2016). CRY2 and FBXL3 cooperatively degrade c-MYC. Mol. Cell *64*, 774–789.

Janich, P., Toufighi, K., Solanas, G., Luis, N.M., Minkwitz, S., Serrano, L., Lehner, B., and Benitah, S.A. (2013). Human epidermal stem cell function is regulated by circadian oscillations. Cell Stem Cell *13*, 745–753.

Janich, P., Meng, Q.J., and Benitah, S.A. (2014). Circadian control of tissue homeostasis and adult stem cells. Curr. Opin. Cell Biol. *31*, 8–15.

Kasof, G.M., Goyal, L., and White, E. (1999). Btf, a novel death-promoting transcriptional repressor that interacts with Bcl-2-related proteins. Mol. Cell. Biol. *19*, 4390–4404.

Khan, S.K., Xu, H., Ukai-Tadenuma, M., Burton, B., Wang, Y., Ueda, H.R., and Liu, A.C. (2012). Identification of a novel cryptochrome differentiating domain required for feedback repression in circadian clock function. J. Biol. Chem. *287*, 25917–25926.

Kim, J.H., Jin, P., Duan, R., and Chen, E.H. (2015). Mechanisms of myoblast fusion during muscle development. Curr. Opin. Genet. Dev. *32*, 162–170.

Koike, N., Yoo, S.H., Huang, H.C., Kumar, V., Lee, C., Kim, T.K., and Takahashi, J.S. (2012). Transcriptional architecture and chromatin landscape of the core circadian clock in mammals. Science *338*, 349–354.

Kriebs, A., Jordan, S.D., Soto, E., Henriksson, E., Sandate, C.R., Vaughan, M.E., Chan, A.B., Duglan, D., Papp, S.J., Huber, A.L., et al. (2017). Circadian repressors CRY1 and CRY2 broadly interact with nuclear receptors and modulate transcriptional activity. Proc. Natl. Acad. Sci. USA *114*, 8776–8781.

Lee, J.E., Lee, J.Y., Wilusz, J., Tian, B., and Wilusz, C.J. (2010). Systematic analysis of cis-elements in unstable mRNAs demonstrates that CUGBP1 is a key regulator of mRNA decay in muscle cells. PLoS ONE *5*, e11201.

Lefta, M., Wolff, G., and Esser, K.A. (2011). Circadian rhythms, the molecular clock, and skeletal muscle. Curr. Top. Dev. Biol. *96*, 231–271.

Lin, K.K., Kumar, V., Geyfman, M., Chudova, D., Ihler, A.T., Smyth, P., Paus, R., Takahashi, J.S., and Andersen, B. (2009). Circadian clock genes contribute to the regulation of hair follicle cycling. PLoS Genet. *5*, e1000573.

Lowrey, P.L., and Takahashi, J.S. (2011). Genetics of circadian rhythms in Mammalian model organisms. Adv. Genet. *74*, 175–230.

Maeda, Y., Fujimura, L., O-Wang, J., Hatano, M., Sakamoto, A., Arima, M., Ebara, M., Ino, H., Yamashita, T., Saisho, H., and Tokuhisa, T. (2006). Role of Clast1 in development of cerebellar granule cells. Brain Res. *1104*, 18–26.

McPherson, J.P., Sarras, H., Lemmers, B., Tamblyn, L., Migon, E., Matysiak-Zablocki, E., Hakem, A., Azami, S.A., Cardoso, R., Fish, J., et al. (2009). Essential role for Bclaf1 in lung development and immune system function. Cell Death Differ. *16*, 331–339.

Menet, J.S., Rodriguez, J., Abruzzi, K.C., and Rosbash, M. (2012). Nascent-Seq reveals novel features of mouse circadian transcriptional regulation. eLife *1*, e00011.

Millay, D.P., O'Rourke, J.R., Sutherland, L.B., Bezprozvannaya, S., Shelton, J.M., Bassel-Duby, R., and Olson, E.N. (2013). Myomaker is a membrane activator of myoblast fusion and muscle formation. Nature *499*, 301–305.

Millay, D.P., Gamage, D.G., Quinn, M.E., Min, Y.L., Mitani, Y., Bassel-Duby, R., and Olson, E.N. (2016). Structure-function analysis of myomaker domains required for myoblast fusion. Proc. Natl. Acad. Sci. USA *113*, 2116–2121.

Motohashi, N., and Asakura, A. (2014). Muscle satellite cell heterogeneity and self-renewal. Front. Cell Dev. Biol. *2*, 1.

Oster, H., Yasui, A., van der Horst, G.T., and Albrecht, U. (2002). Disruption of mCry2 restores circadian rhythmicity in mPer2 mutant mice. Genes Dev. *16*, 2633–2638.

Pizarro, A., Hayer, K., Lahens, N.F., and Hogenesch, J.B. (2013). CircaDB: a database of mammalian circadian gene expression profiles. Nucleic Acids Res. *41*, D1009–D1013.

Plikus, M.V., Van Spyk, E.N., Pham, K., Geyfman, M., Kumar, V., Takahashi, J.S., and Andersen, B. (2015). The circadian clock in skin: implications for adult stem cells, tissue regeneration, cancer, aging, and immunity. J. Biol. Rhythms *30*, 163–182.

Preußner, M., and Heyd, F. (2016). Post-transcriptional control of the mammalian circadian clock: implications for health and disease. Pflugers Arch. *468*, 983–991.

Saini, J., McPhee, J.S., Al-Dabbagh, S., Stewart, C.E., and Al-Shanti, N. (2016). Regenerative function of immune system: Modulation of muscle stem cells. Ageing Res. Rev. *27*, 67–76.

Sarras, H., Alizadeh Azami, S., and McPherson, J.P. (2010). In search of a function for BCLAF1. Sci. World J. *10*, 1450–1461.

Shepard, P.J., and Hertel, K.J. (2009). The SR protein family. Genome Biol. *10*, 242.

Soták, M., Sumová, A., and Pácha, J. (2014). Cross-talk between the circadian clock and the cell cycle in cancer. Ann. Med. *46*, 221–232.

Takahashi, J.S. (2017). Transcriptional architecture of the mammalian circadian clock. Nat. Rev. Genet. *18*, 164–179.

Thresher, R.J., Vitaterna, M.H., Miyamoto, Y., Kazantsev, A., Hsu, D.S., Petit, C., Selby, C.P., Dawut, L., Smithies, O., Takahashi, J.S., and Sancar, A. (1998). Role of mouse cryptochrome blue-light photoreceptor in circadian photoresponses. Science *282*, 1490–1494.

van der Horst, G.T., Muijtjens, M., Kobayashi, K., Takano, R., Kanno, S., Takao, M., de Wit, J., Verkerk, A., Eker, A.P., van Leenen, D., et al. (1999). Mammalian Cry1 and Cry2 are essential for maintenance of circadian rhythms. Nature *398*, 627–630.

Vitaterna, M.H., Selby, C.P., Todo, T., Niwa, H., Thompson, C., Fruechte, E.M., Hitomi, K., Thresher, R.J., Ishikawa, T., Miyazaki, J., et al. (1999). Differential regulation of mammalian period genes and circadian rhythmicity by cryptochromes 1 and 2. Proc. Natl. Acad. Sci. USA *96*, 12114–12119.

Walsh, K., and Perlman, H. (1997). Cell cycle exit upon myogenic differentiation. Curr. Opin. Genet. Dev. *7*, 597–602.

Zuccolo, J., Bau, J., Childs, S.J., Goss, G.G., Sensen, C.W., and Deans, J.P. (2010). Phylogenetic analysis of the MS4A and TMEM176 gene families. PLoS ONE *5*, e9369.

Cell Reports, Volume *22*

Supplemental Information

Cry2 Is Critical for Circadian Regulation of Myogenic Differentiation by Bclaf1-Mediated mRNA Stabilization of Cyclin D1 and Tmem176b

Matthew Lowe, Jacob Lage, Ellen Paatela, Dane Munson, Reilly Hostager, Ce Yuan, Nobuko Katoku-Kikyo, Mercedes Ruiz-Estevez, Yoko Asakura, James Staats, Mulan Qahar, Michaela Lohman, Atsushi Asakura, and Nobuaki Kikyo

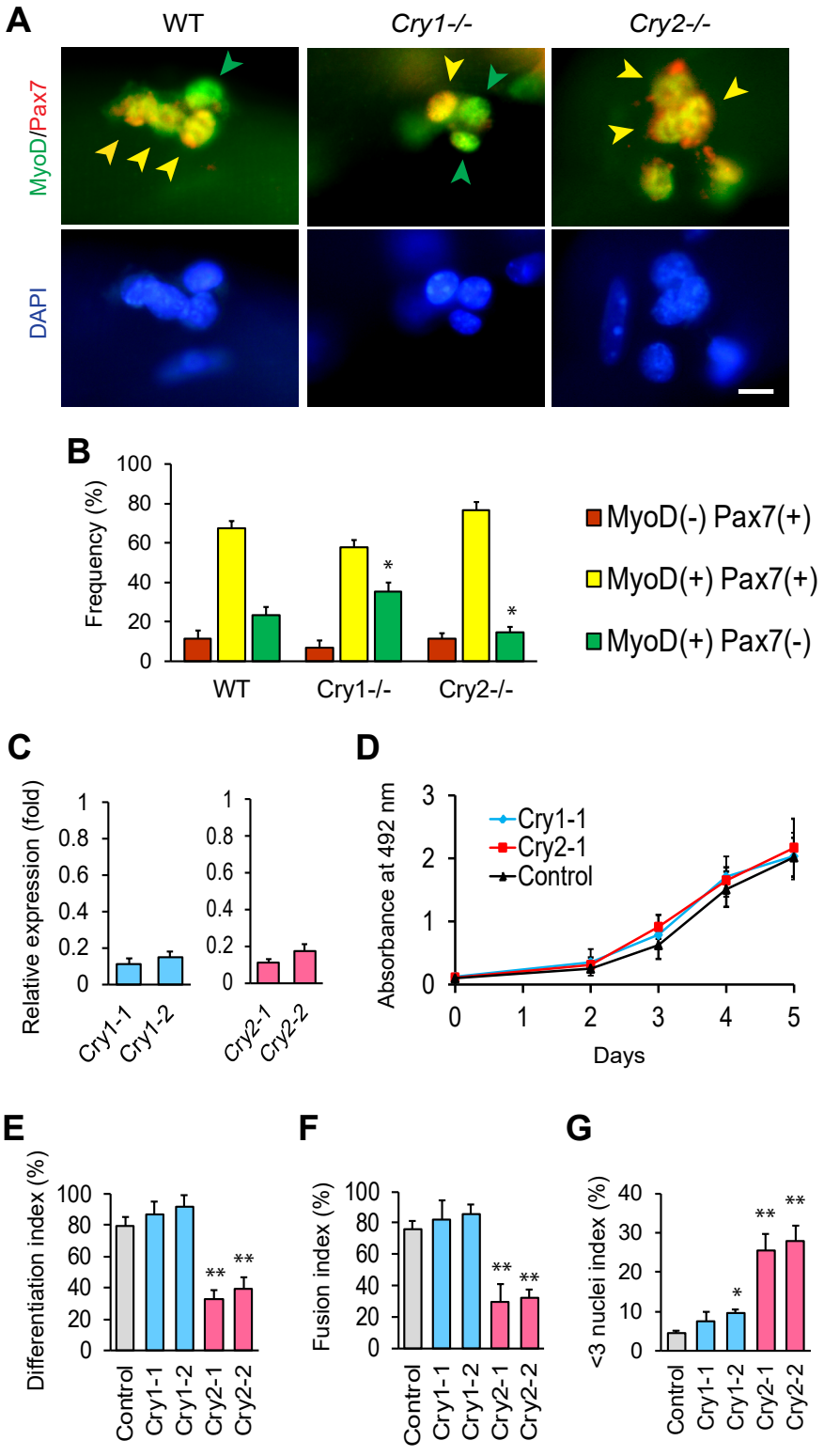
A
WT
Cry1-/-
Cry2-/-
MyoD/Pax7
DAPI
B
Frequency (%)
100
80
60
40
20
0
WT
Cry1-/-
Cry2-/-
MyoD(-) Pax7(+)
MyoD(+) Pax7(+)
MyoD(+) Pax7(-)
C
Relative expression (fold)
1
0.8
0.6
0.4
0.2
0
Cry1-1
Cry1-2
Cry2-1
Cry2-2
D
Absorbance at 492 nm
3
2
1
0
Cry1-1
Cry2-1
Control
0
1
2
3
4
5
Days
E
Differentiation index (%)
100
80
60
40
20
0
**
**
Control
Cry1-1
Cry1-2
Cry2-1
Cry2-2
F
Fusion index (%)
100
80
60
40
20
0
**
**
Control
Cry1-1
Cry1-2
Cry2-1
Cry2-2
G
<3 nuclei index (%)
40
30
20
10
0
*
**
**
Control
Cry1-1
Cry1-2
Cry2-1
Cry2-2

Figure S1. Single muscle culture and KD of *Cry1* and *Cry2* in C2C12 cells, Related to Figures 2 and 3.

(A) Immunofluorescence staining of single muscle fibers with antibodies against MyoD (green) and Pax7 (red) after culture for 72 hr. MyoD(+)Pax7(+) myoblasts and MyoD(+)Pax7(-) differentiating muscle cells are indicated by yellow and green arrow heads, respectively. Satellite cells differentiate from MyoD(-)Pax7(+) to MyoD(+)Pax7(+) and subsequently to MyoD(+)Pax7(-). Scale bars, 10 μm.

(B) Frequency of MyoD(-)Pax7(+), MyoD(+)Pax7(+), and MyoD(+)Pax7(-) cells per cluster in muscle fibers after 72 hr of culture. Nuclei were counterstained with DAPI. * $p < 0.05$ vs WT in each experiment.

(C) Verification of *Cry1* and *Cry2* KD with two shRNA clones each, as determined by qRT-PCR. Values obtained with scrambled control shRNA were defined as 1.0 for each gene.

(D) MTS assay reflecting the proliferation of undifferentiated C2C12 cells after KD. Cell number and absorbance at 492 nm were proportional in this range.

(E-G) Differentiation index (C), fusion index (D), and <3 nuclei index (E) of KD cells on differentiation day 5 after seeding 50% more cells than in the experiments shown in Figure 3.

* $p < 0.05$ and ** $p < 0.01$ with Student's t-test in comparison to control cells in (D) – (F). Data are presented as mean + or ± SD.

A

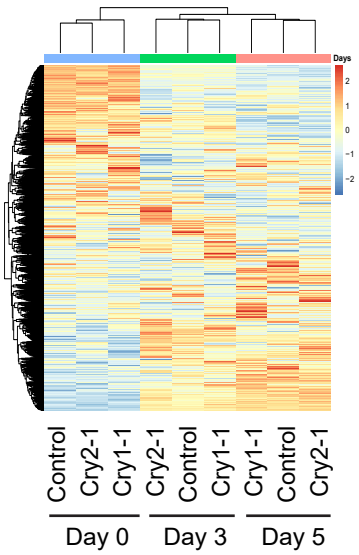

B

Day	GO.biological.process.complete	GO Term	Q-value
Common to Cry1 knockdown and Cry2 knockdown			
Day 0	positive regulation of gene expression	GO:0010628	0.158
Day 3	negative regulation of cellular process	GO:0048523	0.0291
	negative regulation of biological process	GO:0048519	0.0294
	sensory perception of smell	GO:0007608	0.0513
	regulation of response to stimulus	GO:0048583	0.0925
Day 5	biological process	GO:0008150	0.00291
	sensory perception of smell	GO:0007608	0.0662
Unique to Cry1 knockdown			
Day 0	muscle contraction	GO:0006936	1.39E-10
	muscle system process	GO:0003012	2.43E-10
	striated muscle contraction	GO:0006941	1.14E-09
	muscle structure development	GO:0061061	1.69E-08
	single-multicellular organism process	GO:0044707	2.11E-08
Day 3	single-multicellular organism process	GO:0044707	2.09E-07
	single-organism process	GO:0044699	6.72E-07
	single-organism developmental process	GO:0044767	1.03E-06
	sensory perception of smell	GO:0007608	1.69E-06
	developmental process	GO:0032502	2.18E-06
Day 5	sensory perception of smell	GO:0007608	2.86E-07
	sensory perception of chemical stimulus	GO:0007606	3.83E-07
	positive regulation of biological process	GO:0048518	3.69E-06
	regulation of protein phosphorylation	GO:0001932	9.61E-06
	regulation of phosphate metabolic process	GO:0019220	1.23E-05
Unique to Cry2 knockdown			
Day 0	sensory perception of chemical stimulus	GO:0007606	2.48E-06
	sensory perception of smell	GO:0007608	1.61E-05
	neurological system process	GO:0050877	0.0197
	sensory perception	GO:0007600	0.0477
	anatomical structure development	GO:0048856	0.182
Day 3	sensory perception of chemical stimulus	GO:0007606	3.63E-09
	nitrogen compound metabolic process	GO:0006807	5.2E-08
	small molecule metabolic process	GO:0044281	5.05E-07
	cellular metabolic process	GO:0044237	5.81E-07
	cellular aromatic compound metabolic process	GO:0006725	1.67E-06
Day 5	negative regulation of biological process	GO:0048519	1.05E-09
	negative regulation of cellular process	GO:0048523	4.69E-09
	regulation of multicellular organismal process	GO:0051239	5.42E-08
	single-multicellular organism process	GO:0044707	2.9E-07
	regulation of metabolic process	GO:0019222	3.2E-07

C

Gene Name	Cry1 KD d0	Cry2 KD d0	Control
Pdgfb	3.64414	1.42597	1.28925
Srpk3	2.4738	0.0837234	0.389264
Mef2c	9.9333	5.45377	4.73853
Tmem8c	56.0597	19.4364	25.9513
Tnnc2	52.5134	15.4048	22.5019
Unc45b	3.21806	0.622719	1.0898
Myh3	28.8923	7.92271	10.9988
Asb2	1.62383	0.143142	0.739527
Fos	2.89222	2.11009	1.07484
Myom1	2.15062	0.584248	0.553912
Sox8	4.89027	3.39345	2.02162
Ankrd2	3.16961	0.497477	0.749631
Rnf165	1.03459	0.884614	0.229971
Chrng	45.0611	18.1336	13.4901
Tnni1	119.275	29.1413	40.3591
Myog	126.857	24.8798	41.552
Neb	5.92033	2.20951	1.87545
P2ry1	1.20066	0.0873125	0.157887
Casq2	21.2917	4.76115	8.21436
Col11a1	1.16825	0.268703	0.114478
Myoz2	2.64201	0.608452	0.577949
Lmod2	3.82104	1.09149	1.74595
Csrp3	4.21602	0	0.597977
Ryr1	4.36259	1.46478	1.67789
Mylpf	677.864	228.075	235.661
Tnni2	71.386	26.2358	30.7181
Acta1	264.395	52.8698	85.2098
Heyl	29.1419	17.574	9.30169
Sgcg	9.99904	3.48892	3.9587
Alpk3	1.14383	0.574932	0.349444
Smpx	6.42495	0.855687	0.773644
Mybph	46.0292	13.6283	18.2709
Trim72	6.44429	2.2691	1.67293
Lmod3	6.33085	2.6638	2.9436
Klhl31	1.20681	0.520883	0.577973
Eid2	2.50605	1.87726	1.24466
Ttn	3.41562	2.42825	1.41645
Actn2	1.4499	0.219203	0.545036
Smyd1	14.1181	5.32254	5.83401
Myh8	1.00322	0.1002	0.216463
Myh1	7.50119	0.866544	1.50278
Ryr3	1.32927	0.146207	0.327331
Mkx	1.49487	0	0.258782
Tnnt3	88.5619	24.2797	33.3768
Myl1	227.385	67.2128	74.6497
Tnnt1	70.8799	24.237	33.7336
Actc1	61.7528	10.8975	19.8112
Klhl40	4.51323	1.4545	1.55414
Klhl41	12.5266	4.67286	3.64608
Tnnc1	141.333	39.551	57.4244

D

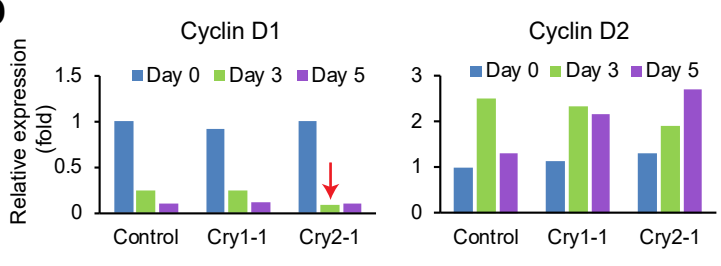

E

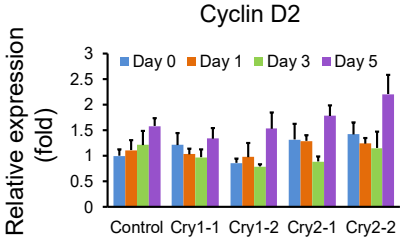

Figure S2. RNA-seq analysis of the KD cells, Related to Figure 4.

(A) Heat map comparing the transcriptome of KD cells.
(B) Enriched GO terms in each segment of the Venn diagram shown in Figure 4A. The GO terms mentioned in the text are highlighted in yellow.
(C) Genes belonging to the highlighted GO terms from the day 0 *Cry1* KD in (B). The FPKM (Fragments per Kilobase of Exon per Million Fragments Mapped) was compared between *Cry1* KD, *Cry2* KD, and control cells. The genes mentioned in the text are highlighted in yellow.
(D) Relative expression levels of cyclin D1 and cyclin D2 obtained from the RNA-seq data. The value with control cells on day 0 was defined as 1.0. The arrow indicates the data mentioned in the text.
(E) qRT-PCR results comparing the expression levels of *Ccnd2* during differentiation of KD cells. The value obtained with control on day 0 was defined as 1.0. Data are presented as mean + SD.

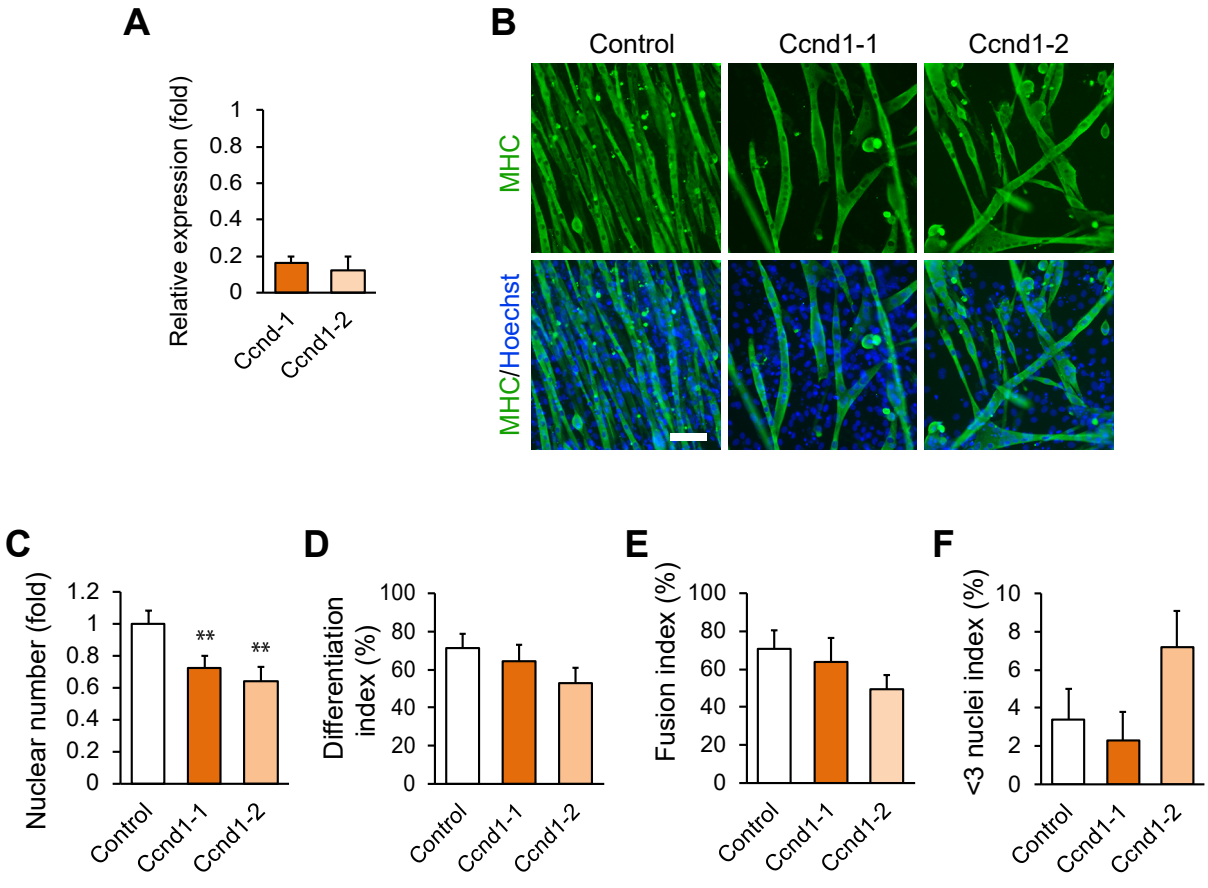
A
Relative expression (fold)
1
0.8
0.6
0.4
0.2
0
Ccnd-1
Ccnd1-2
B
Control
Ccnd1-1
Ccnd1-2
MHC
MHC/Hoechst
C
Nuclear number (fold)
1.2
1
0.8
0.6
0.4
0.2
0
**
**
Control
Ccnd1-1
Ccnd1-2
D
Differentiation index (%)
100
80
60
40
20
0
Control
Ccnd1-1
Ccnd1-2
E
Fusion index (%)
100
80
60
40
20
0
Control
Ccnd1-1
Ccnd1-2
F
<3 nuclei index (%)
10
8
6
4
2
0
Control
Ccnd1-1
Ccnd1-2

Figure S3. Differentiation of C2C12 cells after KD of *Ccnd1*, Related to Figure 4.

(A) Relative expression level of *Ccnd1* in C2C12 cells after KD with two shRNA clones. The value obtained with the control shRNA was defined as 1.0.
(B) MHC staining of KD cells with two different shRNA clones on differentiation day 5. Bar, 100 μm
(C) Nuclear number of KD cells on differentiation day 5. The number with control shRNA was defined as 1.0.
(D-F) Differentiation index (D), fusion index (E), and <3 nuclei index (F) of *Ccnd1* KD cells on differentiation day 5.
** $p < 0.01$ with Student's t-test in comparison to control cells. Data are presented as mean + SD.

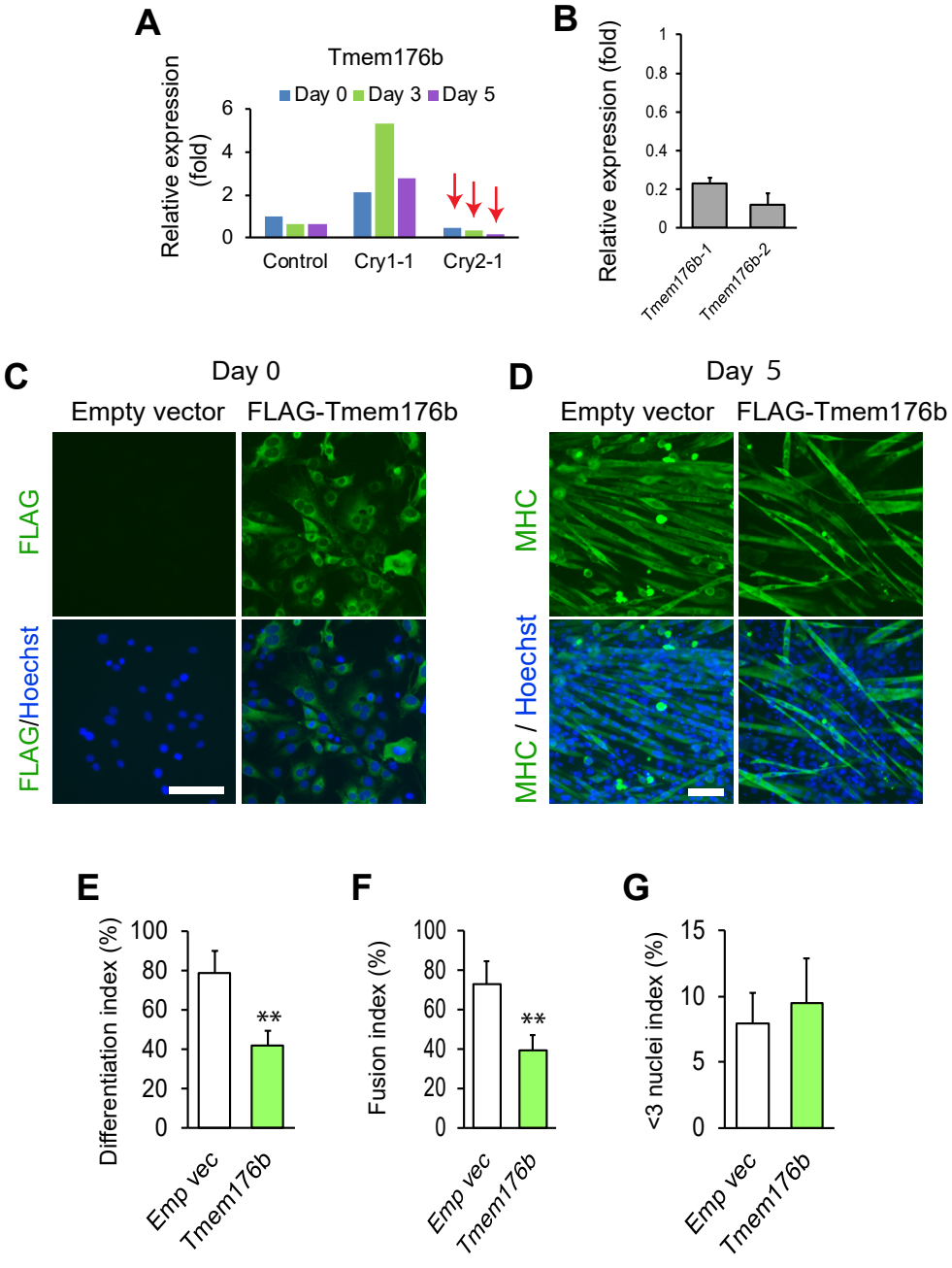
A
Tmem176b
Day 0
Day 3
Day 5
Relative expression (fold)
6
4
2
0
Control
Cry1-1
Cry2-1
B
Relative expression (fold)
1
0.8
0.6
0.4
0.2
0
Tmem176b-1
Tmem176b-2
C
Day 0
Empty vector
FLAG-Tmem176b
FLAG
FLAG/Hoechst
D
Day 5
Empty vector
FLAG-Tmem176b
MHC
MHC / Hoechst
E
Differentiation index (%)
100
80
60
40
20
0
**
Emp vec
Tmem176b
F
Fusion index (%)
100
80
60
40
20
0
**
Emp vec
Tmem176b
G
<3 nuclei index (%)
15
10
5
0
Emp vec
Tmem176b

Figure S4. Characterization of Tmem176b in C2C12 cells, Related to Figure 5.

(A) Relative expression levels of *Tmem176b* in *Cry1* and *Cry2* KD cells. The values were obtained from the RNA-seq data. The value with control cells on day 0 was defined as 1.0. The arrows indicate the data mentioned in the text.
(B) Relative expression level of *Tmem176b* in C2C12 cells after KD with two shRNA clones. The value obtained with the control shRNA was defined as 1.0.
(C) Immunofluorescence staining of the FLAG tag in undifferentiated C2C12 cells transduced with FLAG-Tmem176b. Bar, 100 μm.
(D) Immunofluorescence staining of the FLAG tag in day 5 differentiated C2C12 cells transduced with FLAG-Tmem176b. Bar, 100 μm.
(E-G) Differentiation index (E), fusion index (F), and <3 nuclei index (G) of cells transduced with empty vector or *Tmem176b* cDNA on differentiation day 5.
** $p < 0.01$ with Student's t-test in comparison to the empty vector data. Data are presented as mean + SD in (B), (E), (F), and (G).

A

FLAG-Cry1-binding proteins

Accession	Coverage (%)	#Peptides	#Unique	Description
gi|126157504	10	22	22	serine/arginine repetitive matrix protein 2
gi|6752954	58	21	1	actin cytoplasmic 2
gi|22094119	9	18	18	unconventional myosin-XVIIIa
gi|6681031	18	13	7	cryptochrome-1 (Cry1)
gi|8394460	18	6	6	tropomodulin-3
gi|254587962	20	5	5	serine/threonine-protein phosphatase PGAM5 mitochondrial
gi|31981690	9	5	4	heat shock cognate 71 kDa protein
gi|329755241	8	7	7	gelsolin
gi|114326446	2	4	4	myosin-9
gi|19527344	8	3	3	serine/threonine-protein kinase 38
gi|33620739	22	3	3	myosin light polypeptide 6
gi|165905585	6	4	4	LIM domain and actin-binding
gi|33598964	2	3	3	myosin-10
gi|9845257	17	2	2	histone H1.2
gi|29789070	5	2	2	F-box/LRR-repeat protein 3 (Fbxl3)
gi|254540166	5	3	2	78 kDa glucose-regulated protein precursor
gi|226823279	1	2	2	period circadian protein homolog 1 (Per1)

B

FLAG-Cry2-binding proteins

Accession	Coverage (%)	#Peptides	#Unique	Description
gi|126157504	17	36	36	serine/arginine repetitive matrix protein 2
gi|157823889	34	17	3	actin gamma-enteric smooth muscle
gi|439253893	33	17	3	actin alpha skeletal muscle
gi|27312016	44	25	20	cryptochrome-2 (Cry2)
gi|22094119	15	31	31	unconventional myosin-XVIIIa
gi|226823279	9	10	10	period circadian protein homolog 1 (Per1)
gi|33598964	8	14	13	myosin-10
gi|114326446	4	7	6	myosin-9 isoform 1
gi|31981690	15	8	4	heat shock cognate 71 kDa protein
gi|8394460	20	7	7	tropomodulin-3
gi|19527344	22	9	9	serine/threonine-protein kinase 38
gi|165905585	10	6	6	LIM domain and actin-binding protein 1
gi|9845257	21	3	3	histone H1.2
gi|33620739	36	5	5	myosin light polypeptide 6
gi|165932375	7	2	2	plasminogen activator inhibitor 1 RNA-binding protein
gi|254587962	12	3	3	serine/threonine-protein phosphatase PGAM5 mitochondrial
gi|240849436	7	3	3	nexilin
gi|29789070	9	3	3	F-box/LRR-repeat protein 3 (Fbxl3)
gi|70906447	4	4	4	bcl-2-associated transcription factor 1 (Bclaf1)
gi|162461907	6	3	3	stress-70 protein mitochondrial
gi|68533246	5	3	3	thyroid hormone receptor-associated protein 3
gi|190194418	1	2	2	desmoplakin
gi|20544149	7	3	2	casein kinase I isoform delta (CK1δ)

C

Bclaf1 gi70906447

303 - TITPQNAPR

303 - TITPQNAPREESR

535 - MIASDSHRPEVK

620 - SPAVTLNER

D

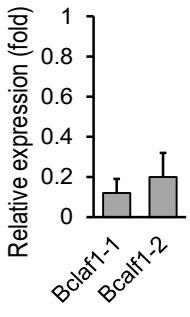

E

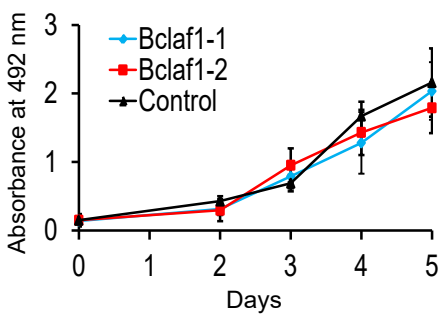

Figure S5. Immunoprecipitation of Cry1- and Cry2-interacting proteins from C2C12 cells, Related to Figure 6.

(A-B) Lists of proteins co-precipitated with FLAG-Cry1 (A) and FLAG-Cry2 (B). Proteins in which more than one peptide sequences were detected are listed. Known circadian regulators are highlighted in red. Bclaf1 is highlighted in yellow in (B). We adjusted peptide false discovery rate (FDR) to 0.5% and protein FDR to 1.0%.

(C) Detected peptide sequences of Bclaf1. The first peptide is a partial sequence of the second one. Amino acid number of the first residue in each peptide is written on the left.

(D) Relative expression levels of *Bclaf1* in KD cells.

(E) MTS assay of *Bclaf1* KD cells.

Data are presented as mean + or ± SD.

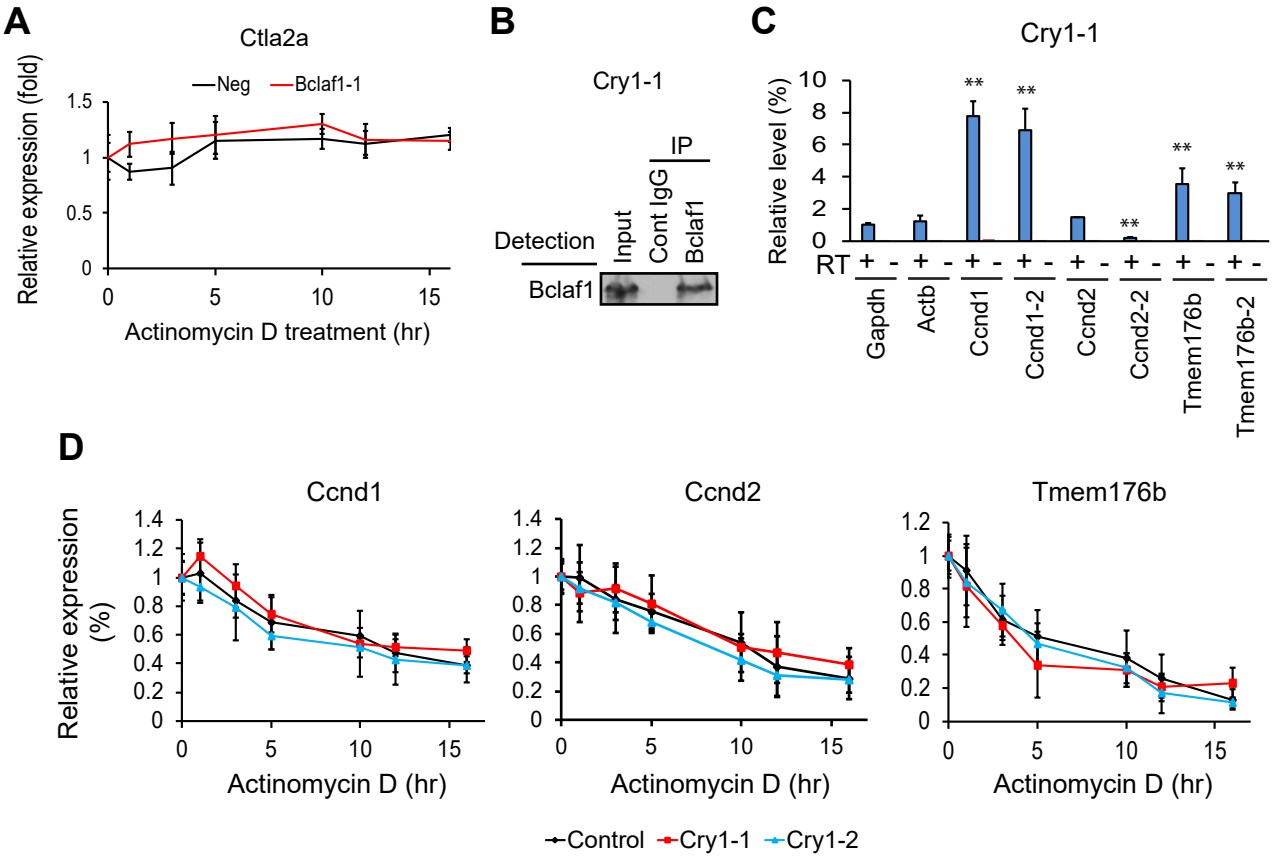
A
Ctla2a
Neg
Bclaf1-1
Relative expression (fold)
Actinomycin D treatment (hr)
B
Cry1-1
IP
Detection
Input
Cont IgG
Bclaf1
Bclaf1
C
Cry1-1
Relative level (%)
RT
Gapdh
Actb
Ccnd1
Ccnd1-2
Ccnd2
Ccnd2-2
Tmem176b
Tmem176b-2
D
Ccnd1
Ccnd2
Tmem176b
Relative expression (%)
Actinomycin D (hr)
Control
Cry1-1
Cry1-2

Figure S6. *Cry1* KD does not affect Bclaf1-mediated mRNA stabilization, Related to Figure 7.

(A) Relative expression levels of *Ctla2a* in *Bclaf1* KD cells treated with actinomycin D. Data are presented as mean ± SD. The value at 0 hr was defined as 1.0 for each cell type.
(B) Western blotting of immunoprecipitated Bclaf1 from differentiation day 3 of *Cry1* KD cells.
(C) Relative expression levels of mRNAs in the co-immunoprecipitated material with a Bclaf1 antibody. Results with and without reverse transcription (RT) are shown. Two PCR primer sets were used for *Ccnd1*, *Ccnd2*, and *Tmem176b*.
(D) Relative expression levels of three mRNAs in *Cry1* KD cells treated with actinomycin D. The expression levels were normalized against *Ctla2a* mRNA at each time point and subsequently against 0 hr for each gene.
** $p < 0.01$ with Student's t-test in comparison to control cells. Data are presented as mean + or ± SD.

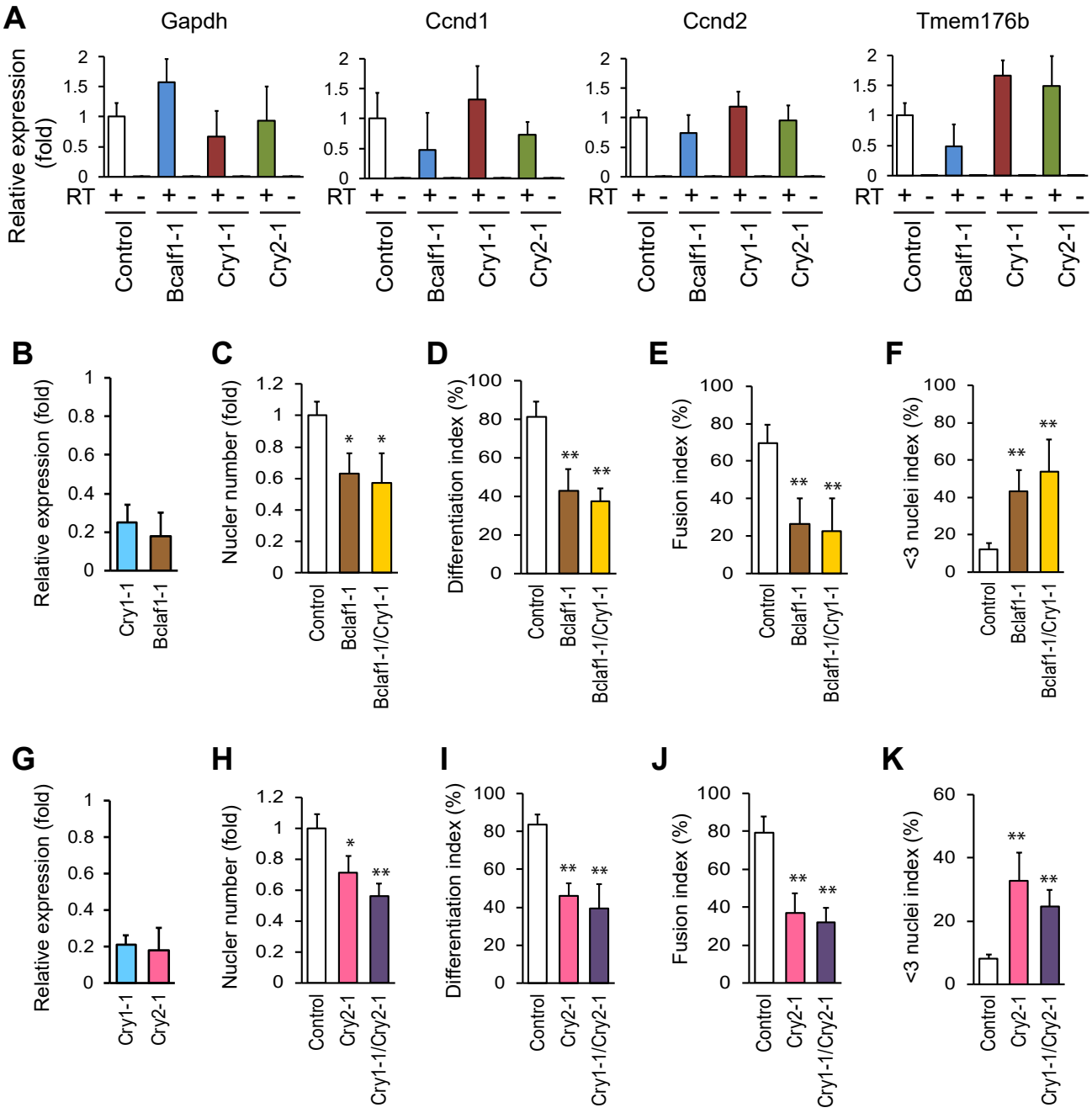
A
Gapdh
Ccnd1
Ccnd2
Tmem176b
Relative expression (fold)
RT
Control
Bcalf1-1
Cry1-1
Cry2-1
B
Relative expression (fold)
Cry1-1
Bclaf1-1
C
Nucler number (fold)
Control
Bclaf1-1
Bclaf1-1/Cry1-1
D
Differentiation index (%)
E
Fusion index (%)
F
<3 nuclei index (%)
G
Relative expression (fold)
Cry1-1
Cry2-1
H
Nucler number (fold)
Control
Cry2-1
Cry1-1/Cry2-1
I
Differentiation index (%)
J
Fusion index (%)
K
<3 nuclei index (%)

Figure S7. Effects of *Cry1*, *Cry2*, and *Bclaf1* KD on myoblast differentiation, Related to Figure 7.

(A) qRT-PCR of nascent mRNAs. Results with (+) and without (-) reverse transcription (RT) are shown.
(B) Relative expression levels of *Cry1* and *Bclaf1* in double KD cells.
(C) Nuclear numbers in *Bclaf1* KD and *Bclaf1/Cry1* double KD cells on differentiation day 5.
(D-F) Differentiation index (D), fusion index (E), and <3 nuclei index (F) in *Bclaf1* KD and *Bclaf1/Cry1* double KD cells on day 5.
(G) Relative expression levels of *Cry1* and *Cry2* in double KD cells.
(H) Nuclear numbers comparing *Cry2* KD and *Cry1*/*Cry2* double KD cells on day 5.
(I-K) Differentiation index (I), fusion index (J), and <3 nuclei index (K) comparing *Cry2* KD and double KD cells on day 5.
* $p < 0.05$ and ** $p < 0.01$ with Student's t-test in comparison to control cells. Data are presented as mean + SD.

Table S1. shRNA clones, Related to Experimental Procedures

Gene	Manufacturer	Catalog #
Control	Sigma-Aldrich	SHC016-1EA
Cry1-1	GE Life Sciences	TRCN0000176255
Cry1-2	GE Life Sciences	TRCN0000173610
Cry2-1	Sigma-Aldrich	TRCN0000240548
Cry2-2	Sigma-Aldrich	TRCN0000194121
Ccnd1-1	GE Life Sciences	TRCN0000026948
Ccnd1-2	GE Life Sciences	TRCN0000026881
Tmem176b-1	GE Life Sciences	TRCN0000105305
Tmem176b-2	GE Life Sciences	TRCN0000105306
Bclaf1-1	GE Life Sciences	TRCN0000084413
Bclaf1-2	GE Life Sciences	TRCN0000084416

Table S2. Sequences of qPCR primers, Related to Experimental Procedures

Gene	Forward	Reverse
MyoD	TGAGCAAAGTGAATGAGGCCTTCG	TGCAGACCTTCGATGTAGCGGAT
Myogenin (*Myog*)	CCCTATTTCTACCAGGAGCCCCAC	GCGCAGGATCTCCACTTTAGGCAG
Myomaker (*Mymk*)	ATCGCTACCAAGAGGCGTT	CACAGCACAGACAAACCAGG
MHC (*Myh3*)	CACCTGGAGAGGATGAAGAAGAA	AAGACTTGACTTTCACTTGGAGTTTATC
Ckm	CTCAGCAAGCACAACAATCAC	GATGACATCGTCCAGAGTGAAG
Gapdh	TGCACCACCAACTGCTTAG	GATGCAGGGATGATGTTC
Ccnd1	CAGAGGCGGATGAGAACAAG	GAGGGTGGGTTGGAAATGAA
Ccnd1-2	GCCGAGAAGTTGTGCATCTA	AGGTTCCACTTGAGCTTGTT
Ccnd2	CTCCCGCAGTGTTCCTATTT	TCACAGACCTCTAGCATCCA
Ccnd2-2	CAGGAGCTGCTGGAGTGGGAACTG	AACTTGAAGTCGGTAGCGC
Tmem176b	CCTGGAGATTGTTGTGTCTGT	AGCTTCCTCTCTGACTCTTCT
Tmem176b-2	GCAAACCAGTGTTCCCTACT	ATCATCACTGTATCGCACTGTC
Bmal1	CAACCCATACACAGAAGCAAAC	CATCTGCTGCCCTGAGAATTA
Per1	CAGGATGTGGGTGTCTTCTATG	GTGAAGTCCTTGAGACCTGAAC
Cry1	CTCAGTCCTTATCTCCGCTTTG	CCACAGGAGTTGCCCATAAA
Cry2	GATGCCGATTTCAGTGTGAATG	GGCAGTAGCAGTGGAAGAAT
Bclaf1	ACACAGAGGAGACAGAGGATTA	CTCAGTATTCCGGTGAGATGAAG
Ctla2a	GGCAAGACCAGCTTCTACAT	CAGGAGCCATTTCTCCTCTATTC
Actb	GAGGTATCCTGACCCTGAAGTA	CACACGCAGCTCATTGTAGA

Supplemental Experimental Procedures

Knockout Mice

Cry1$^{+/-}$ mice (B6.129P2-Cry1^{tm1Asn}/J, stock # 016186) and *Cry2*$^{+/-}$ mice (B6.129P2-Cry2^{tm1Asn}/J, stock# 016185) were purchased from Jackson Laboratory. Genotyping to detect the mutated *Cry1* and *Cry2* alleles was performed by PCR using the primers described on the web site of Jackson Laboratory. Age-matched littermate wild type (WT) mice were used as controls. Mice were housed in a specific pathogen free (SPF) environment and were monitored by the Research Animal Resources (RAR) staff of the University of Minnesota. Mice were provided access to drinking water and standard chow ad libitum under a 14 hr-light and 10 hr-dark cycles except for the 12 hr-light and 12 hr-dark experiments to isolate TA muscles described below. Mice were euthanized by CO_2 inhalation or KCl injection after anesthesia with 2-4% isoflurane (Phoenix). These methods are consistent with the recommendations of the Panel of Euthanasia of the American Veterinary Medical Association.

Culture of C2C12 cells

Mouse myoblast C2C12 cells were purchased from American Type Culture Collection (ATCC, CRL-1772) and maintained with 10% FBS in DMEM in an incubator at 37°C with 5% CO_2. Differentiation was induced as follows. On day -2, cells were seeded at $1x10^5$ cells/well in a 12-well plate. On day 0 the wells became confluent. The cells were rinsed twice with phosphate buffered saline (PBS) and cultured with 1% insulin-transferrin-selenium (ITS) in DMEM. Medium was changed with fresh DMEM with ITS every two days.

Synchronization of Circadian Rhythms of Undifferentiated and Proliferating C2C12 Cells

C2C12 cells were seeded at $8x10^4$ cells/well in a 12-well plate in 10% FBS in DMEM on day -1. On day 1, 10 μM forskolin was added between -1 and 0 hrs. Cells were washed with PBS twice and fresh 10% FBS in DMEM was added at 0 hr. Cells were harvested for qRT-PCR or fixed with 4% formaldehyde for immunofluorescence staining every 4 hrs for 44 hrs. In addition, cells were pulse-labelled with 0.5 μM EdU (5-ethynyl-2'-deoxyuruidine) with a Click-iT EdU Alexa Fluor 448 imaging kit (Invitrogen, C10337) for 30 min before each 4 hr time point.

Synchronization of Circadian Rhythms of Differentiating C2C12 Cells

C2C12 cells were seeded at $1x10^5$ cells/well in a 12-well plate in 10% FBS in DMEM on day -2. On day 0, forskolin was added between -1 and 0 hrs. Cells were washed with PBS twice and then differentiation was started with 5% horse serum (HS) in DMEM at 0 hr. Synchronization was maintained better with HS than with ITS. Cells were harvested for qRT-PCR, fixed for immunofluorescence staining, or treated with EdU as described above every 4 hrs for 120 hrs. Only a half of medium was replaced at 60 hr to preserve circadian rhythms.

MTS Cell Proliferation Assay

C2C12 cells were seeded at $1x10^3$ cells/well in a 96-well plate. On the day of measurement, 20 μl of MTS solution (Promega, CellTiter 96 Aqueous One Solution Cell Proliferation Assay, G3581) was added to 100 μl of culture in each well. After incubation for 2 hr at 37°C, absorbance at 492 nm was measured with an LD400 spectrophotometer (Beckman Coulter). The value obtained from blank wells without cells were subtracted from the absorbance values. Average $\pm$ SD was obtained from three independent experiments.

Circadian Gene Expression in TA Muscles

WT, *Cry1*$^{-/-}$, and *Cry2*$^{-/-}$ male mice aged 8-12 weeks old were entrained at 12hr-light and 12hr-dark cycles (6:00-18:00 light and 18:00-6:00 dark) for two weeks before experiments. This means that Zeitgeber Time 0 (ZT0) corresponds to 6:00 and ZT12, 18:00. TA muscles were isolated every 4 hr starting at ZT2. Total RNA was isolated with a Direct-zol RNA MiniPrep with TRI-Reagent (Zymo Research, R2015). qRT-PCR was performed as described above with two TA muscles each.

Muscle Injury

Male mice of 6-8 weeks old were anesthetized using 2-4% isoflurane. We injected 50 μl 1.2% $BaCl_2$ in 0.9% NaCl into the left TA muscle of four WT, *Cry1*$^{-/-}$, and *Cry2*$^{-/-}$ mice each between ZT4 and ZT8 when *Cry1* and *Cry2* mRNA levels were low. This was because peak timing of these mRNA levels was different among WT, *Cry1*$^{-/-}$, and *Cry2*$^{-/-}$ mice (Fig. 4C), leaving the lower timing more consistent. Mice were euthanized 3, 4, 5, and 7 days post injection and the TA muscle was extracted between ZT4 and ZT8. Cryosections with a thickness of 10 μm were prepared for immunofluorescence, Hematoxylin Eosin (HE), and Sirius red staining.

Preparation of Primary Myoblasts
Satellite cell-derived primary myoblasts were obtained from adult hind limb muscle of 2-month-old WT, *Cry1*$^{-/-}$, and *Cry2*$^{-/-}$ mice as described previously (Motohashi et al., 2014). Briefly, muscles were minced and digested with collagenase type 2 (Worthington, CLS-2) to obtain dissociated muscle cells. Satellite cells were then purified with MS columns (Miltenyi Biotec, 130-042-201) and LD columns (Miltenyi Biotec, 130-042-901) by negative selection with antibodies against CD31-PE (eBioscience, 12-0311), CD45-PE (eBioscience, 12-0451), and Sca1-PE (eBioscience, 12-5981), followed by anti-PE MicroBeads (Miltenyi Biotec, 130-048-801). This was followed by positive selection with an antibody against biotin-conjugated integrin α7-biotin (Miltenyi Biotec, 130-102-125) and anti-biotin MicroBeads (Miltenyi Biotec, 130-090-485). Isolated satellite cells were cultured on dishes coated with rat tail collagen (BD Biosciences, 354236) in myoblast growth medium consisting of HAM's F-10 medium with 20% fetal bovine serum (FBS), 10 ng/ml basic fibroblast growth factor (bFGF) (Invitrogen, PHG0263), penicillin (100 U/ml), and streptomycin (100 mg/ml) at 37°C with 5% CO_2. Low- passage satellite cell-derived primary myoblasts (typically less than eight passages) were used for immunostaining. Differentiation medium (Dulbecco's Modified Eagle Medium (DMEM) supplemented with 5% HS, penicillin, and streptomycin) was used for myogenic differentiation.

Gene Knockdown
293FT cells (Invitrogen, R70007) were seeded at $3x10^5$ cells/well in a 12-well plate with 10% FBS in DMEM on day 1. Cells were transfected with a 0.5 μg pLKO.1 vector encoding an shRNA sequence (GE Life Science, Table S1) along with 0.2 μg each of pCMV-VSV-G (Addgene, 8454), pRSV-Rev (Addgene, 12253), and pMDLg/pRRE (Addgene, 12251) with 2.75 μl Lipofectamine 2000 (Invitrogen, 11668019) on day 2. Culture medium was replaced with fresh DMEM with 10% FBS 5 hr later. On day 5 the medium containing lentivirus was harvested and filtered through a 0.45 μm syringe filter. C2C12 cells that had been seeded in 12-well plates on day 4 were transduced with 400 μl of the virus suspension with 0.8 μg/ml polybrene (Sigma, H9268) and 400 μl DMEM with 10% FBS. Culture medium was replaced with fresh DMEM with 10% FBS on day 6. Virus-integrated cells were selected with 1 μg/ml puromycin dihydrochloride (MB Bio, 100552) between days 7 and 14. The proliferated cells were frozen in liquid nitrogen or used in differentiation studies.

Gene Subcloning
The FUW-tetO-hOCT4 (FUW) vector used was obtained from Addgene (20726). The zeocin resistance gene was replaced with a puromycin resistance gene. The FUW vector was further modified with the removal of the *hOCT4* sequence. Additionally, an adaptor with the restriction sites PacI, EcoRI, and BamHI was subcloned into the EcoRI site of FUW. The Flag x3-Linker sequence shown below were obtained from GeneArt (Invitrogen) and amplified from their pcDNA3 vector and subcloned into FUW.
Flag x3-Linker
GAATTCATGGACTACAAGGACGACGACGACAAGGATTACAAGGATGATGATGATAAGGACTATAAGG
ACGATGATGACAAAGGCGGCGGAGGCAGCGGATCCCTCGAG

The *Tmem176b* gene were amplified from cDNA prepared from C2C12 cells and inserted into the BamHI site at the 3' side of the linker in the FUW-Flag x3-Linker vector using the Gibson method.

Gene Overexpression
The FUW-tetO-FLAG-Tmem176b vector was transfected into 293FT cells to prepare lentivirus as described above. The FUW vector and FUW-M2rtTA (Addgene 20342) were used at 0.25 μg each in place of the pLKO.1 vector. Tetracyclin-free FBS was used to prevent premature induction of the transgenes. C2C12 cells were transduced as described above to establish cell lines. The transgenes were induced with 2 μg/ml doxycycline for four days before use for immunofluorescence staining and immunoprecipitation.

Actinomycin D Treatment
Cells were treated with 5 μg/ml actinomycin D (Sigma-Aldrich, A1410) for 17 hr to arrest transcription to study the stability of mRNA. Ctla2a was used as control mRNA due to its long half-life (687 min) in C2C12 cells (Lee et al., 2010).

Immunofluorescence Staining of C2C12 Cells
Transduced C2C12 cells were fixed with 4% paraformaldehyde for 15 min on day 3 and 5 during differentiation and

permeabilized with 0.5% Triton X-100 in PBS for 5 min. Cells were then incubated with the antibody against myosin heavy chain (MHC, Developmental Studies Hybridoma Bank, MF20, 1:200 dilution) and the secondary antibody Alexa Fluor 488 goat anti-mouse IgG (H+L) (Thermo Fisher Scientific, A11029, 1:200 dilution) for 1 hr each at 25°C. DNA was counterstained with 5 μg/ml Hoechst 33342 (Sigma, B2261). Fluorescence signal was captured with a LUCPlanFLN 20x objective lens (Olympus) with 0.45 Ph1 aperture and a C11440-42U digital camera (Hamamatsu) attached to an IX73P2F microscope (Olympus). Adobe Photoshop CS6 was used for image processing. Differentiation index was defined as a percentage of nuclei (Hoechst-stained structure) existing within MHC(+) cells among 1,000 nuclei in total. Fusion index is a percentage of nuclei located in MHC(+) cells that contained two or more nuclei in each cell among the same 1,000 nuclei. <3 nuclei index is a percentage of nuclei that were located in MHC(+) cells containing one or two nuclei among all MHC(+) cell nuclei.

Immunofluorescence Staining of Primary Myoblasts

Cells were fixed with 2% formaldehyde and were blocked with 1% bovine serum albumin in PBS. Cells were then stained with anti-MyoD (Santa Cruz Biotechnology, sc-760, 1:200 dilution) and anti-MHC antibodies. After staining, they were incubated with the secondary antibodies Alexa Fluor 488 donkey anti-mouse IgG (Thermo Fisher Scientific, A21202, 1:200 dilution) and Alexa Fluor 594 donkey anti-rabbit IgG (Thermo Fisher Scientific, A21207, 1:200 dilution). DNA were counterstained with 4',6'-diamidine-2'-phenylindole dihydrochloride (DAPI, 10236276001).

Single Muscle Fiber Culture and Immunostaining

Single muscle fibers were isolated by 0.2% collagenase type I digestion (Sigma-Aldrich, C0130) of extensor digitorum longus muscles for 90 min at 37 ºC. Isolated single muscle fibers were transferred and cultured on 5% HS-coated tissue culture dishes with DMEM supplemented with 10% HS and 1% chicken embryo extract (MP Biomedicals, 092850145) for 72 hr. Single muscle fibers were fixed with 2% paraformaldehyde in PBS for 20 min, permeabilized with 0.2% Triton X-100 in PBS for 10 min, and blocked with 10% bovine serum albumin in PBS for 30 min. The fibers were stained with primary antibodies (anti-Pax7, Developmental Studies Hybridoma Bank, 1:5 and anti-MyoD, Santa Cruz Biotechnology, sc-304, 1:500) and secondary antibodies (Alexa Fluor 488 donkey anti-rabbit IgG (H+L), Thermo Fisher Scientific, A21206, 1:500 and Alexa Fluor 568 donkey anti-mouse IgG (H+L), Thermo Fisher Scientific, A10037, 1:500). Nuclei were counterstained with DAPI.

Staining of EdU Uptake

EdU uptake was assessed by pulse labeling C2C12 cells with 0.5 μM EdU for 30 min, followed by fixation with 4% formaldehyde and detection with a Click-iT EdU Alexa Fluor 448 imaging kit following the instructions provided by the manufacturer. Frequency of EdU uptake was calculated by observing 1,000 nuclei.

Western Blotting

Protein transferred to an Immobilon P membrane (Millipore Sigma, IPVH00010) was detected with primary antibodies against FLAG (Sigma, F1804, 1:200 dilution), Cry1 (Alpha Diagnostic International, CRY11-A, 1:200 dilution), Cry2 (Alpha Diagnostic International, CRY12-A, 1:200 dilution), and Bclaf1 (Bethyl Laboratory, A300-608A, 1:200 dilution) with mouse anti-rabbit IgG-HRP light chain specific (Jackson ImmunoResearch 211-032-171, 1:1000 dilution), goat anti-rabbit IgG-HRP (Santa Cruz Biotechnology sc-2004, 1:1000 dilution), and goat anti-mouse IgG-HRP (Santa Cruz Biotechnology, sc-2005, 1:1000 dilution). The chemiluminescence signal was detected with a SuperSignal West Dura kit (Thermo Fisher Scientific, 34075) and X-ray films.

Quantitative RT-PCR (qRT-PCR)

RNA was isolated from cells with a Quick-RNA MiniPrep kit (Zymo Research, R1055). cDNA was synthesized using 1.0 μg of total RNA with ProtoScript II First Strand cDNA Synthesis Kit (NEB, E6560L) and random hexamers. Real-time quantitative PCR was performed using a GoTaq qPCR Master Mix (Promega, A6002) in a 96-well PCR plate in a Mastercycler realplex^2 thermocycler (Eppendorf). Primer sequences are listed in Table S2. mRNA expression levels were analyzed by normalizing expression values to glyceraldehyde 3-phosphate dehydrogenase (*Gapdh*) expression. Mean ± SD of three independent experiments were calculated.

Immunofluorescence Staining of TA Sections

Sections were first fixed with 2% paraformaldehyde for 10 min, followed by permeabilization with 0.2% Triton X-100 in PBS for 5 min. The sections were treated with two blocking reagents: 3% Mouse-on-Mouse Blocking Reagent (Vector MKB-2213) in PBS for 1 hr and 5% FBS in PBS for 30 min. Mouse anti-embryonic myosin heavy chain (eMHC, Developmental Studies Hybridoma Bank, F1.652-f, 1:5 dilution) and rabbit anti-laminin (Sigma, L9393,

1:2000 dilution) antibodies were used as primary antibodies diluted in 5% FBS in PBS. After 1 hr incubation, sections were washed twice with 0.01% Triton-X100 in PBS. The secondary antibodies Alexa Fluor 488 goat anti-mouse IgG (H+L) (Thermo Fisher Scientific, A11029, 1:200 dilution) and Alexa Fluor 555 goat anti-rabbit IgG (H+L) (Thermo Fisher Scientific, A21429, 1:200 dilution) diluted in 5% FBS in PBS were used along with 5 μg/ml Hoechst 33342 (Sigma, B2261) for 1 hr. Sections were mounted using Fluorescent Mounting Medium (DAKO, S302380-2). Fluorescence images were captured using Metamorph Basic software (Molecular Devices) and an ORCA-flash4.0LT camera (Hamamatsu) attached to an IX73 microscope (Olympus) with a 20X LUCPlan FL N lens. Images were processed with Photoshop and Illustrator CS6 (Adobe).

Hematoxylin Eosin (HE) Staining

Sections were first fixed using 2% formaldehyde for 5 min. Sections were then treated as follows: deionized water for 1 min, Harris Modified Hematoxylin (Thermo Fisher Scientific, SH26-500D) for 2 min, tap water for 1 min, deionized water for 1 min, Eosin-Y (Thermo Fisher Scientific, 22-220-104) for 5 min, 95% ethanol for 30 sec, 100% ethanol for 2 min twice, and xylene for 10 min twice. Sections were mounted using Permount (Thermo Fisher Scientific, SP15-100). Images were captured with cellSens Entry 1.11 software (Olympus) and a DP26 camera (Olympus) attached to the microscope described above.

Sirius Red Staining

The Sirius red solution was made as 1% Direct Red 80 in 1.3% picric acid. TA sections were fixed with acetone, pre-chilled at -20°C, for 10 min. The sections were then washed in deionized water for 1 min, stained with Sirius red for 15 min, and rinsed with 0.5% acetic acid for 1 min. The sections were subsequently washed with 100% ethanol for 2 min and twice with xylene for 10 min. Finally, the sections were mounted with Permount for taking images as described for HE staining. Quantifications were done using the entire section area with ImageJ (Shimizu-Motohashi et al., 2015).

Immunoprecipitation

Whole cell extracts were prepared by resuspending $4x10^6$ cells with 300 μl lysis buffer (50 mM Tris-HCl pH8.0, 150 mM NaCl, 2 mM $MgCl_2$, 1% NP40, 0.1 mM phenylmethylsulfonyl fluoride, 2 mM leupeptin, 1.5mM pepstatin A, and 150 u/ml benzonase). The extracts were incubated for 30 min at 25°C with 5 μl Dynabeads Protein G (Thermo Fisher Scientific, 10004D) that had been washed with 0.1% Tween 20 in PBS and then loaded with 3 μg of anti-FLAG M2 monoclonal antibody (Sigma F1804) or normal mouse IgG (Santa Cruz Biotechnology, sc-2025). After incubation the beads were washed three times with 500 μl of 0.1% Tween 20 in PBS. Bound proteins were eluted by incubation with 30 μl of 100 μg/ml 3X FLAG peptides (Sigma, F4799) in PBS with 0.1% Tween 20 for 10 min on ice. Elution was repeated three times in total and they were combined for mass spectrometry or western blotting.

Endogenous Cry1, Cry2, and Bclaf1 were immunoprecipitated with the antibodies described above. Co-precipitated proteins were eluted by incubating the beads in 30 μl of 1X Laemmli buffer (50 mM Tris-HCl, pH6.8, 2% SDS, 10% glycerol, 0.005% bromophenol blue, and 25 mM dithiothreitol) at 95°C for 5 min. Eluted proteins were applied to SDS-PAGE for western blotting.

Mass Spectrometry

Proteins eluted from Dynabeads Protein G were run into a Criterion 8-16% Tris-HCl gradient gel (Bio-Rad Laboratories, 3450038) for 25 min at 25 mA constant current. The gel was fixed with 40% ethanol and 10% acetic acid for 30 min and then stained with Imperial Protein Stain (Thermo Fisher Scientific, 24615). The stained protein regions were excised and in-gel trypsin digestion was performed (Shevchenko et al., 1996). The dried peptide mixtures were solubilized in 2% acetonitrile and 0.1% trifluoroacetic acid in water and cleaned with the Stage Tip protocol (Rappsilber et al., 2003) and dried in vacuo.

Approximately 1.5 μg of sample was injected for a mass spectrometry analysis. Spectra were acquired on an Orbitrap Fusion (Thermo Fisher Scientific) coupled to an Easy-nLC 1000 (Thermo Fisher Scientific) ultrahigh pressure liquid chromatography pump. Peptides were separated on an in-house packed 100 μm internal diameter, 20 cm column containing ReproSil-Pur C18 resin (3μm, 120 Å, Dr. Maisch GmbH, Germany). Liquid chromatography solvents employed were 0.1% formic acid in water (A) and 0.1% formic acid in acetonitrile (B) with a gradient consisting of 2 min of 2-8% B, 40 min of 8-30% B, 1 min of 30-90% B, 5 min of 90% B, 1 min of 90-2% B, and 5 min of 2% B with a flow rate of 330 nl/min.

Mass spectrometric data was acquired in top 8 data dependent mode. The MS1 spectra data was collected at a resolution of 60,000, with an automated gain control (AGC) target of 400,000 and a max injection time of 50 ms.

Precursor ions were filtered according to charge state (2-7 *z*) and an intensity of >130,000 were selected for MS/MS, in which a dynamic exclusion window of 10 seconds and ± 10 ppm mass accuracy was employed for previously examined precursor ions. Isolation of MS2 precursor ions was performed using a quadruple mass filter set to 1.6 *m/z* window and fragmentation of precursor ions was performed using an HCD-normalized collision energy of 35 with first mass set to 100 *m/z*. The MS/MS scan was acquired with Orbitrap resolution of 15,000, an AGC target of 50,000, and a maximal injection time of 100 milliseconds.

RNA Immunoprecipitation

RNA immunoprecipitation was performed with an EZ-Magna RIP RNA-binding protein immunoprecipitation kit (Millipore Sigma, 17-701) following the instruction. Non-crosslinked cell extract was prepared from $1x10^7$ non-transduced C2C12 cells on differentiation day 3 with the kit. Bclaf1was immunoprecipitated with 5 µg of anti-Bclaf1 antibody (Bethyl Laboratory, A300-608A) for 4 hr at 4°C. Normal rabbit IgG (Santa Cruz Biotechnology, sc-2027) was used as a control. Purified RNA was applied to qRT-PCR as described above.

qPCR analysis of nascent mRNAs

Nascent RNA was pulse-labeled with 5-ethynyl uridine for 1 hr, biotinylated, and purified with streptavidin magnetic beads with a Click-iT Nascent RNA kit (Thermo Fisher Scientific, C10365). RT-qPCR was performed as described above.

RNA-Seq

1) Sample Quality Assessment

Total RNA was prepared from KD C2C12 cells before differentiation (day 0) and day 3 and 5 during differentiation. shRNA clone #1 was used for Cry1 and Cry2 KD. Total RNA isolates were quantified with a Quant-iT RiboGreen RNA Assay Kit (Thermo Fisher Scientific, R11490). RNA integrity was assessed by generating an RNA Integrity Number (RIN) with capillary electrophoresis using a BioAnalyzer 2100 (Agilent). All samples passed the initial quality control, having over 1 µg of RNA and RIN over 8.

2) Library creation: Samples were converted to Illumina sequencing libraries using a Truseq RNA Sample Preparation Kit (Illumina, RS-122-2001). Briefly, polyA (+) RNA was purified from 1 µg total RNA with oligo-dT-coated magnetic beads, fragmented, and reverse-transcribed into cDNA. The cDNA was further fragmented, blunt-ended, and ligated to indexed (barcoded) adaptors and amplified with 15 cycles of PCR. Final library size distribution was validated with capillary electrophoresis and quantified with a Quant-iT PicoGreen dsDNA Assay Kit (Thermo Fisher Scientific, P11496) and quantitative PCR. Indexed libraries were then normalized, pooled, and size-selected to 320 bp ± 5% with a LabChip XT (PerkinElmer).

3) Cluster generation and sequencing: Libraries were hybridized to a single read flow cell and individual fragments were clonally amplified by bridge amplification on a cBot (Illumina). Once clustering was completed, the flow cell was loaded onto a HiSeq 2500 (Illumina) and sequenced using Illumina's SBS chemistry. Upon completion of read 1, an 8 bp forward and 8 bp reverse (i7 and i5) index read was performed.

4) Primary analysis and de-multiplexing: Base call (.bcl) files for each cycle of sequencing were generated by Real Time Analysis (RTA) software (Illumina, https://support.illumina.com/downloads/hcs-2-2-68.html). The base call files and run folders were then exported to servers maintained at the Minnesota Supercomputing Institute (MSI). Primary analysis and de-multiplexing were performed using bcl2fatstq software version 2.17.1.14 (Illumina, https://support.illumina.com/sequencing/sequencing_software/bcl2fastq-conversion-software.html). The de-multiplexed FASTQ files were used for subsequent analyses.

5) Sequence analysis: Over 5 million reads were generated per library and the average quality score passing quality filter were above Q30. Raw sequences were analyzed using a customized pipeline (gopher-pipelines; https://bitbucket.org/jgarbe/gopher-pipelines/overview) developed and maintained by the MSI. Briefly, quality controls were performed on each FASTQ files using FastQC version 0.11.5 (http://www.bioinformatics.babraham.ac.uk/projects/fastqc/) before and after adapter trimming with Trimmomatic version 0.33 (http://www.usadellab.org/cms/index.php?page=trimmomatic) (Bolger et al., 2014). Post-trimming sequences were aligned to GRCm38/mm10 reference genome using HISAT2 version 2.0.2 (https://ccb.jhu.edu/software/hisat2/index.shtml) (Kim et al., 2015). Transcript abundance was then estimated using subread version 1.4.6 (http://subread.sourceforge.net/) (Liao et al., 2014).

Differential gene expression was determined using Cufflinks version 2.2.1 (http://cole-trapnell-lab.github.io/cufflinks/) (Trapnell et al., 2012). Pathway analysis of differentially expressed genes were performed by functionally annotate the genes and perform overrepresentation enrichment test using PANTHER (http://pantherdb.org/) (Mi et al., 2013).

6) Heat maps: Heat maps were generated using *DESeq2* (Version 1.10.1, http://www.bioconductor.org/packages/release/bioc/html/DESeq2.html) and *pheatmap* version 1.0.8 (https://cran.r-project.org/web/packages/pheatmap/index.html) packages in R version 3.2.3 (https://www.r-project.org/) (Love et al., 2014). Briefly, read counts generated by subread are filtered to include genes with at least 5 reads in at least 1 sample. The remaining reads were then log transformed. Heat maps were generated using the log transformed values with *pheatmap* package. Hierarchical clustering was performed using euclidian distances and average linkage clustering method.

QUANTIFICATION

Image analysis

For TA muscle sections stained for eMHC, randomly selected 2,000 myofibers from two mice totaling 4,000 myofibers from each strain were used in the histograms in Figure 1C and in the statistical analysis. The pixels depicting myofibers expressing eMHC were classified as foreground and everything else as background. These images were then made binary and the area of each myofiber was found with ImageJ (NIH). These areas were then sorted based on size to make a histogram.

For the HE-stained sections, randomly selected 500 myofibers with centrally located nuclei from four mice totaling 2,000 myofibers for each mouse strain are shown in the histograms in Figures 1E and 1G and were used in statistical analysis. Cross section images of myofibers were separated using the Pixel Classification program of the ilastik 1.2 software (ilastik). The pixels depicting myofibers with centrally located nuclei were classified as foreground and everything else as background. ImageJ was then used to make these images binary and to find the cross-sectional area of the myofibers. Myofibers were then sorted based on size to make histograms. The raw number of myofibers within each size range was divided by the total number of myofibers to give the frequency, which is shown in Figures 1C, 1E, and 1G.

Supplemental References

Bolger, A.M., Lohse, M., and Usadel, B. (2014). Trimmomatic: a flexible trimmer for Illumina sequence data. Bioinformatics *30*, 2114-2120.

Kim, D., Langmead, B., and Salzberg, S.L. (2015). HISAT: a fast spliced aligner with low memory requirements. Nat Methods *12*, 357-360.

Lee, J.E., Lee, J.Y., Wilusz, J., Tian, B., and Wilusz, C.J. (2010). Systematic analysis of cis-elements in unstable mRNAs demonstrates that CUGBP1 is a key regulator of mRNA decay in muscle cells. PLoS One *5*, e11201.

Liao, Y., Smyth, G.K., and Shi, W. (2014). featureCounts: an efficient general purpose program for assigning sequence reads to genomic features. Bioinformatics *30*, 923-930.

Love, M.I., Huber, W., and Anders, S. (2014). Moderated estimation of fold change and dispersion for RNA-seq data with DESeq2. Genome Biol *15*, 550.

Mi, H., Muruganujan, A., and Thomas, P.D. (2013). PANTHER in 2013: modeling the evolution of gene function, and other gene attributes, in the context of phylogenetic trees. Nucleic Acids Res *41*, D377-386.

Motohashi, N., Asakura, Y., and Asakura, A. (2014). Isolation, culture, and transplantation of muscle satellite cells. J Vis Exp, doi: 10.3791/50846.

Rappsilber, J., Ishihama, Y., and Mann, M. (2003). Stop and go extraction tips for matrix-assisted laser desorption/ionization, nanoelectrospray, and LC/MS sample pretreatment in proteomics. Anal Chem *75*, 663-670.

Shevchenko, A., Wilm, M., Vorm, O., and Mann, M. (1996). Mass spectrometric sequencing of proteins silver-stained polyacrylamide gels. Anal Chem *68*, 850-858.

Shimizu-Motohashi, Y., Asakura, Y., Motohashi, N., Belur, N.R., Baumrucker, M.G., and Asakura, A. (2015). Pregnancy-induced amelioration of muscular dystrophy phenotype in mdx mice via muscle membrane stabilization effect of glucocorticoid. PLoS One *10*, e0120325.

Trapnell, C., Roberts, A., Goff, L., Pertea, G., Kim, D., Kelley, D.R., Pimentel, H., Salzberg, S.L., Rinn, J.L., and Pachter, L. (2012). Differential gene and transcript expression analysis of RNA-seq experiments with TopHat and Cufflinks. Nat Protoc *7*, 562-578.